A three-dimensional model of the morphogenesis of the rhesus lateral geniculate nucleus.

Svilen Tzonev, Joseph Malpeli, and Klaus Schulten.

Beckman Institute
Technical Report
University of Illinois
1998

1 Structure and Development of the Primate LGN

Each side of the mammalian brain contains a structure called the lateral geniculate nucleus (LGN), which receives visual input from both eyes and sends projections to the primary visual cortex. The cell bodies of several types of retinal ganglion (RG) cells lie on the inside surface of the eyeball. Their axons exit the eyeball through a hole called the optic disk, located in the nasal (closer to the nose) part of the eye. The region in the retina occupied by the disk is devoid of receptor cells, forming the so-called blind spot in the visual field. At the optic chiasm the nerve fibers from both eyes meet, and from there follow a path to the left or right LGN, depending on their origin in the retinas: axons originating from left (right) hemiretina of both eyes proceed towards the left (right) LGN. In this way, each LGN receives input only from the ipsilateral (same-side, as defined by the LGN position in the brain) halves of both retinas, or equivalently, from the contralateral (opposite-side) halves of the visual field[1].

The retinal ganglion cells in primates fall into two classes according to their size: α or M-type have larger size, larger receptive field, higher conducting velocity, and β or P-type have smaller size, smaller receptive fileds and lower conducting velocity. Depending on the structure of their receptive fields, the RG cells are classified also into On and Off type.

In primates, the LGN consists of several distinct layers of neurons separated by intervening layers of axons and dendrites. Projections of a given type of RG cells terminate in one LGN layer. With some exceptions, each layer receives input from only one type of RG cells. In each layer, the retinal projections form a map of the contralateral visual field. All maps are organized in a topographic fashion, i.e., nearby RG cells of the same type project to nearby LGN neurons within a layer (Figure 1).

Figure 2 schematically presents the structure of a rhesus macaque monkey LGN with regions consisting of six, four, and two neuronal layers, and the relationship between these regions and the structure of retinal input. The macaque retinas are not symmetric with respect to the vertical meridian. The nasal (closer to the nose) hemiretina is larger than the temporal (closer

[1]The inverted correspondence between the left (right) visual hemifield and the right (left) hemiretinas is due to the inversion of the image by the eye lenses.

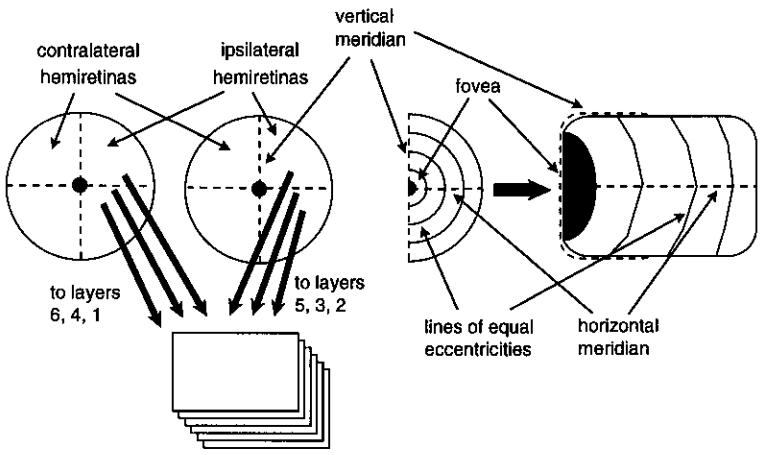

Figure 1: **Left:** The two retinae are divided into ipsilateral (same-side, relative to the position of one LGN) and contralateral (opposite side) hemiretinas, separated by the vertical meridian. The RG cells from the ipsilateral hemiretinas project to the same LGN. The LGN neurons are segregated into distinct layers according to the type of their retinal input. In each layer a topographic map of the corresponding hemiretina is found. **Right:** A close-up view of the map (projections of one RG cell type) between one half of one retina and one LGN layer. The map is neighborhood-preserving. Representations of lines of equal eccentricities and the horizontal meridian are shown in the retina and in the layer, the vertical meridian in the retina is mapped along a part of the edge of the layer. The very central $(1.5-2\,\mathrm{deg})$ part of the retina (the fovea) is shown as a dark area. Its relative expansion in the LGN is due to higher density of retinal ganglion cells in the central retinal region..

to the temples) hemiretina. This leads to the existence of a region in visual space which is mapped by only one eye. This region is viewed only by the contralateral eye and is called the monocular crescent. The rest (more central part) of the visual space is viewed by both eyes.

Because of the retinotopic map between the eyes and the LGN, the boundary between binocular and monocular vision is clearly represented in the LGN as a surface separating portions of the nucleus with four and two cellular layers. On the other hand, the interface between the six- and four-layered parts of the LGN lies entirely within the binocular region of the map, passing through the representation of the optic disk in the LGN[2]. Other than the presence of the optic disk in one hemiretina, there is no other anatomical or physiological change of the retinas at this point, however, the structure of the LGN changes dramatically. The retinotopy in the visual space maps is so rigorous that the optic disk is represented by cell-free spaces, called the optic disk gaps.

An anatomical reconstruction of a rhesus LGN cut along the representation of the horizontal meridian is presented in Figure 3. The layers are numbered ventrally to dorsally (bottom to top in the head). Central vision is represented in the posterior (to the back of the head) part of the LGN (to the left in the figure). The binocular region in the visual space is represented in the six- and four-layered portions, the monocular crescent is mapped in the two-layered portion. The cell-free spaces on the border between the six- and four-layered portions are the representations of the optic disk in the contralateral hemiretina, and are not present in layers mapping the ipsilateral eye.

Based on the body size and type of retinal input, two major classes of LGN neurons and layers can be defined. The cells in layers 1 and 2 are larger and receive input from the M-type RG cells. The layers 1 and 2 and their cells are called magnocellular. The cells in layers 3, 4, 5 and 6 are smaller, and receive input from the P-type RG cells. These four layers and their cells are called parvocellular. Below we will use the short-hand names parvo and magno for the LGN neurons and layers.

The maps of the contralateral visual hemifield in different layers are put together in register: cells in columns running perpendicular to the layers

[2]Note that the optic disks lie in the nasal hemiretinas and, therefore, only the disk in the contralateral eye is represented in a given LGN

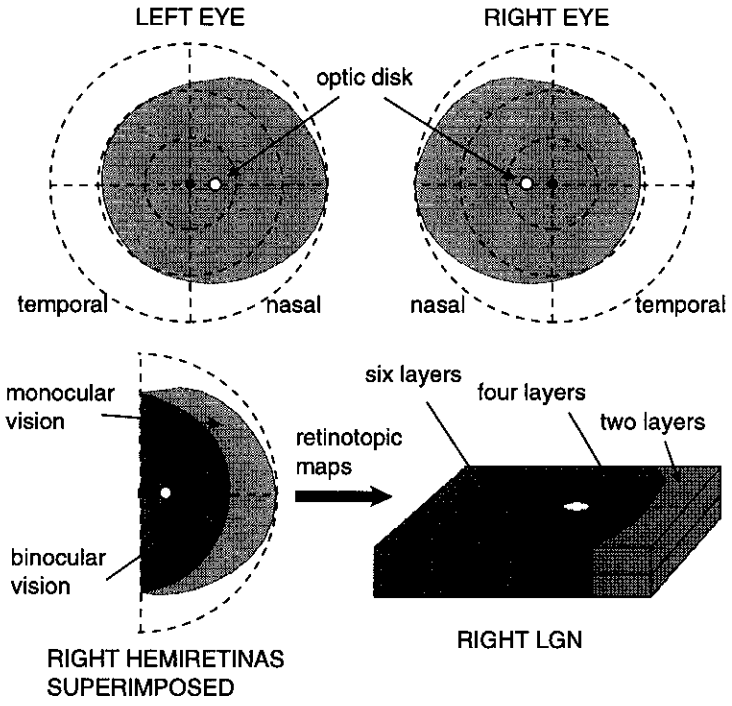

Figure 2: More detailed view of the macaque retinas and LGN. In the upper panels, the actual shapes of the left and right retinas are shown as shaded areas. Note their asymmetric shapes, the nasal (closer to the nose) part of both retinas is larger than the temporal (closer to the temples) part. The optic disk lies on the horizontal meridian in the nasal hemiretinas. The lower left panel shows the right hemiretinas superimposed. Both hemiretinas project to the right LGN. The area of retinal overlap defines the area of binocular vision in the left visual hemifield. The area of monocular vision is where no ipsilateral retina exists. This area is also called monocular crescent . Shaded areas in the LGN (lower right panel) show the representation of the binocular and monocular areas. Portions of the LGN have six, four or two layers of neurons. The transition surface between the four- and two-layered portions corresponds to the boundary between binocular and monocular vision areas. The transition surface between the six- and four-layered portions passes through the representation of the optic disk. Other than the optic disk (which is present only in the contralateral eye!) there is no other anatomical or physiological change in the retinas at this position; the change in the LGN structure, however, is dramatic.

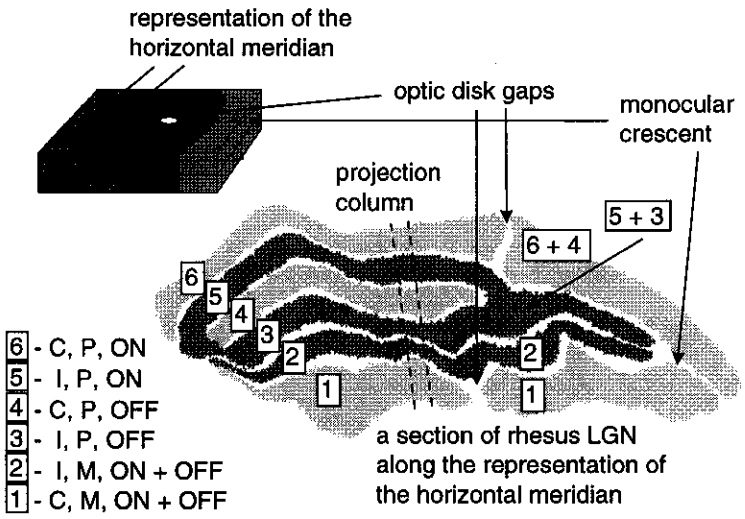

Figure 3: An anatomical reconstruction of a section of rhesus LGN along the representation of the horizontal meridian. The regions with six, four and two neuronal layers are clearly defined. The layers are numbered ventrally-to-dorsally (bottom-to-top in the head). Posterior (back of the head) is to the left. Central vision is mapped in the posterior. The magnocellular layers 1 and 2 contain larger-body neurons, which receive input from the M-type (also larger-body) RG cells. The cells in the parvocellular layers 6, 5, 4, and 3 are smaller and receive input from P-type RG cells. The type of LGN neurons found in varying layers is indicated in the left. The first entry indicates contralateral or ipsilateral eye, the second indicates magno or parvo type, and the third one indicates the polarity of the receptive field. The layers receiving input from the contralateral eye (6, 4 and 1) are shaded lighter. The small cell-free regions in layers 6 and 1 are the representations of the optic disk gap in the contralateral eye. At the position of these gaps layers 6 and 4, and 5 and 3 merge, leading to a four-layered pattern. The magno and parvo cells , and different-eye-input cells remain segregated across the whole nucleus. The parvo cells are segregated into four layers in the central-vision region (ON and OFF types being put separately), the merger at the gaps eliminates physical segregation based on ON/OFF difference but leaves cells with input from different eyes in different layers. Cells in columns running perpendicular to the layers receive input from the same point in the visual field. Neighboring points of the visual field are mapped into neighboring columns.

map the same point of the visual field. An example of this organization is the shape and location of the optic disk gaps, which represent the same hole in the contralateral retina. The retinotopy of all maps ensures that neighboring points in the visual space are mapped into neighboring projection columns. A general organizing principle for the rhesus LGN is that cells of one type are found in only one layer at any given eccentricity. In other words, within a projection column, all eight types of neurons are found, each type being distributed in one cluster, the intersection of the column with the corresponding neuronal layer.

The magno and parvo subsystems are separated everywhere into morphologically distinct layers. The magno subsystem consists of two layers (1 and 2) which differ in their eye specificity: the cells in layer 1 are driven by the contralateral eye, the cells in layer 2 by the ipsilateral eye. ON and OFF polarity cells are not segregated in different layers (see the left panel in Figure 3). The parvo subsystem, however, changes its pattern of lamination at the position of the optic disk gaps. At eccentricities smaller than the optic disk gap (posterior part of the LGN) the four parvo types (C/ON, I/ON, C/OFF, I/OFF) are segregated into four layers (6, 5, 4 and 3, respectively). Anterior to the gaps (where peripheral vision is mapped, to the right in Figure 3), there are two parvo layers (called here 6+4 and 5+3) in which ON and OFF cells from the same eye are not separated by interlaminar space.[3]

The lateral geniculate nucleus first appears as a distinct structure around the tenth gestation week in human [8, 5, 31] and around eighth week in the rhesus macaque monkey [11]. The cluster of precursor cells is initially completely homogenous, and no cellular layers can be seen. Since the retinal ganglion cell axons have not yet made permanent synapses on the future LGN neurons there is nothing to functionally differentiate them from one another. At this stage, even morphological differences between the cells that will develop into magno and parvo classes do not exist [11]. Later in development the axons of the RG cells invade the nucleus and start making synapses on the dendrites of the LGN neurons. Presumably, at this stage the neurons gradually develop their own receptive fields and functionality. It

[3]Some evidence suggests that ON and OFF type cells are clustered into substrata in layers 6+4 and 5+3, ON cells forming the dorsal (upper) substrata. It is conceivable that any repulsion forces are much stronger for different-eye type than for different-polarity type cells, therefore, cells get physically separated from their neighbors only when they are of opposite-eye type.

is also assumed that the process of laminar segregation occurs simultaneously with the maturation of neuronal functionality.

It is important to realize that these developmental processes occur before birth and no external visual input is present. For the higher-order areas of the visual system, in the striate and extrastriate cortex, the presence of normal external visual input is crucial for normal development [15, 21]. Although no external visual input is necessary for the normal LGN development, neural activity in the retinas is. Without proper input from both eyes the LGN fails to develop six layers. If, for example, one eye is removed before birth, the nucleus segregates into only two layers containing the magno and parvo cells [35]. A similar outcome is found for the cat [39].

The process of establishment of mature retinogeniculate connections is spread out in time. In human, the segregation into layers is under way between weeks 22 and 24 gestation age [13]. Data obtained from the Yakovlev Collection in the Armed Forces Institute of Pathology, Washington D.C. suggest that lamination may start as early as week 20. The entire nucleus appears to be laminated by week 24. In the macaque, the lamination appears first between embryonic days 90 and 95 (E90 and E95). It spreads continuously and is completed by E125 to E130 [11]. In both species, human and macaque, an initially homogeneous nucleus gradually acquires its mature lamination pattern. First hints of lamination appear in the part of the LGN which will eventually map the central vision.[4] As time progresses, lamination spreads into parts of the nucleus which will map more and more peripheral areas of the visual field.

The gradual establishment of lamination (at least for the parvo layers) can be described as propagation of a *wave of development.* This wave originates in the central-vision region and within several weeks sweeps across the entire nucleus. Those portions of the LGN through which the wave has passed are in the final laminar pattern; those through which the wave is yet to pass are in a homogeneous, unlaminated state. The propagation of the wave is governed by local cell interactions and is modulated by external morphogenetic gradients, which favor one or another lamination pattern (ordering of the parvo cells within a projection column). The nonuniform development of the

[4]The LGN undergoes extensive solid-body rotation and twisting during the same period of time. The location of the lamination seed rotates about 90 degrees along vertical and horizontal, parallel to the face axes and ends up in the posterior pole of the mature LGN [11, 33].

LGN reflects the nonuniform development of the retina itself. The RG cells and other cells in the retina are known to develop in a central-to-peripheral manner [19]. It is reasonable to assume that the same central-to-peripheral pattern exists in the maturation of the RG cells and their connections with the LGN.

The idea of a gradual spread of a developmental wave is a corner stone in this report. It plays an important role when the dynamics of the suggested model is formulated, as well as when the initial conditions are chosen. It is also essential for the interpretation of the role of optic disk gaps as a local perturbation having a global effect over the state of the whole system. The mechanism through which the gaps have an extended effect is based on the existence of several possible states (laminations) of the system, some of them more stable than others; if at some point (temporal and spatial) of development the system is in a metastable state, even a small perturbation can induce a transition to a more (maybe the most) stable state. The optic disk gaps are suggested to play the role of such a perturbation. Maintenance and propagation of a metastable state are possible because of the imposed restriction for very strict retinotopy during development.

The laminar pattern of the magno subsystem is constant throughout the binocular region despite the optic disk gap in layer 1, which coincides with the transition in the parvo subsystem.. The disappearance of layer 2 in the monocular crescent is trivially explained by the lack of ipsilateral retina for large eccentricities. As a whole, the magno system has a trivial organization and will not be included in the model.

The parvocellular subsystem, however, exhibits a more complicated structure. In the central-vision representation, it is split into four layers: 6, 5, 4 and 3. Each layer consists of parvo cells with particular eye specificity (contra- or ipsilateral) and RF polarity (ON- or OFF-center). The combinations of eye specificity and RF polarity of cells in the parvo layers of the central-vision representation is given in Table 1.

In contrast with the magno subsystem, the parvo subsystem keeps cells with different polarities segregated into different layers for small eccentricities (central vision). For larger eccentricities, the parvo subsystem changes the number of layers and becomes exactly like the magno one: two layers, each mapping one eye, and each having cells with both ON- and OFF-center polarity. The boundary between the 4-layer and 2-layer parvo subsystem passes through the optic disk gaps and extends to the lateral edges of the

	Cell type			
parvo layer #	3	4	5	6
eye dominance	I	C	I	C
center polarity	OFF	OFF	ON	ON

Table 1: Eye specificity and center polarity of cells of the four parvocellular layers in the central-vision portion of the macaque LGN. C denotes contralateral, I ipsilateral; ON or OFF the polarity of the receptive field.

nucleus.

The LGN has three distinct laminar patterns, two in its binocular zone and one in its monocular zone. The laminar pattern in the binocular zone foveal to the optic disk gaps will be called the F pattern (or state). The pattern in the binocular zone peripheral to the gaps will be called the P pattern (or state. In this notation, the F state has four parvo layers (plus two magno layers), the P state has two parvo layers (plus two magno layers). Any other pattern of ordering of parvocellular substrata will be called X pattern.

Evidence presented in [38] suggests that in the P pattern the parvocellular layers 6+4 and 5+3, although not anatomically stratified, preserve some degree of stratification. It appears that cells with ON polarity tend to be found more often in the dorsal (upper) parts of these two layers. Therefore some degree of ordering is preserved in these layers, but this order is not manifested anatomically, it can only be revealed with neurophysiological methods (direct recording of neuronal activity and receptive fields).

The change in the pattern of the parvo layers at the optic disk gaps can be described as a reordering of the strata of parvo cells. Before the gaps (F state) the order is (dorsal to ventral) [6], [5], [4], [3]; after the gaps (P state) it is [6,4], [5,3] . The brackets indicate anatomically segregated layers. The cell strata 4 and 5 have exchanged places. The laminar transition at the gaps is simply a result of reordering of the parvo strata. Presumably, when strata 6 and 4 (or 5 and 3) are next to each other they do not separate anatomically as individual layers because they receive same-eye input. Whenever two cell strata are of opposite eye specificity, though, they are separated as individual layers, as in the F state. If two neighboring strata are of the same eye-specificity and of the same cell type (magno or parvo) they merge as one layer.

Moreover, same-eye magno and parvo strata may merge at large eccentricities (as observed in the human for layers 2 and 3).

There are several possible mechanisms for physical separation of strata given the different functional properties of their cells. One possibility is active cell migration away from cells with opposite-eye specificity, once specificity reaches its mature level. Another possibility is that cells in the initially homogeneous nucleus, which end up between the cores of two strata "disliking" each other, die out, either because of too much competition and opposite pulling interactions, or because they cannot develop pure eye specificity.

2 Model of LGN Morphogenesis

The LGN cells c_i are labeled by indices $i = 1, 2, \ldots, N$ and have fixed, quasi-random and uniformly distributed locations $r_i \in V \subset \Re^3$. For simplicity, we consider a rectangular-shaped nucleus: $V = \{ (x, y, z) \,|\, 0 < x < S_x, 0 < y < S_y, 0 < z < S_z \}$. S_x, S_y and S_z are the dimensions of the bounding box and are chosen in proportion $5 : 3 : 5$, which would be roughly the proportions of a "flattened" macaque nucleus. In reality, the LGN is bent along a middle axis parallel to the x axis, so that points with $y \to 0$ and $y \to S_y$ are closer than in this simplified rectangular model. Each cell belongs to a projection column C_{ab}, $a = 1, 2, \ldots, A$ and $b = 1, 2, \ldots, B$, where $C_{ab} = \{ (x, y, z) \,|\, x \in [(a-1)S_x/A, aS_x/A], y \in [(b-1)S_y/B, bS_y/B], z \in [0, S_z] \}$, see Figure 4.

The projection columns are of the same shape and size. Their number along the x- and y-directions, or, alternatively, their density must be sufficiently high in order to ensure smooth and gradual propagation of development of the neuronal functionality. As a result of development of neuronal functionality, the layers will emerge stacked in the vertical (z-) direction. Foveal vision will be mapped near $x = 0$ and $y = S_y/2$. Peripheral vision will be mapped roughly around the distant half of the lateral edges ($x > S_x/2$ and $y = 0$ or $y = S_y$ and the "peripheral" edge ($x = S_x$), see also Figure 1, right panel.

The cells in this model do not move, their positions are fixed once and for all. This model does not deal with the emergence of the interlaminar space. It is assumed that once the strata are clearly formed they are segregated

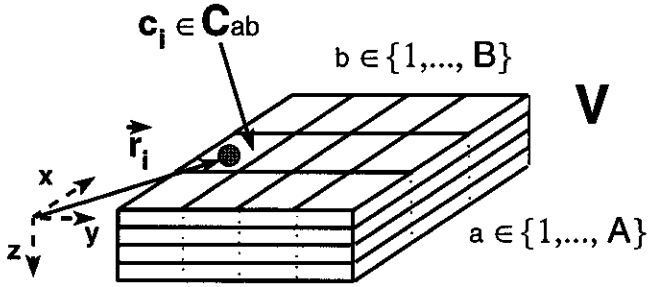

Figure 4: Geometry of the model. LGN cells c_i ($i = 1, 2, \ldots, N$) have fixed random, and uniformly distributed locations r_i within a volume $V \subset \Re^3$, and belong to one projection column C_{ab}.

(following the rules spelled above) by processes of active cell migrations, passive cell migration (cells being pushed away by growing neuronal processes and glial cells), neuronal death on the strata interfaces, or some combination of those processes.

Let the RG cells in the same-side hemiretinas be labeled as g_i, $i = 1, 2, \ldots, M$. Each RG cell[5] is described by five parameters: ρ_i, eccentricity (angular distance from fovea); ϕ_i, elevation from the horizontal meridian; t_i, cell type (P or M); e_i, eye affiliation (contralateral or ipsilateral); and p_i, receptive field polarity (ON or OFF). The first two parameters assume continuous values, while the last three parameters assume discrete ones. Since we are interested only in parvo layer development, the t_i variable can take only one value and will be dropped from consideration.

LGN cells c_j, $j = 1, 2, \ldots, N$, are assigned positions x_i, y_i, and z_i in the nucleus. Each RG cell, g_i, can have multiple synapses on the dendritic tree of any LGN cell. The total strength of such synapses between g_i and c_j is time-dependant and is denoted by $s_{ij}(\tau)$.

Before axons from the RG cells have reached the LGN there are no connections between the retina and the nucleus, and $s_{ij} = 0$ for all i and j. As the RG cell axons arrive in the geniculate and start to form more or less functional synapses with some of the LGN neurons, these neurons begin to acquire some degree of functionality. The outgrowth and retraction of axonal

[5]The number of RG cells projecting to one nucleus is about the same as the number of neurons in the nucleus, i.e., $M \sim N$, but this is not essential in the model.

eye specificity (e)	contalateral	$+1$
	ipsilateral	-1
receptive field polarity (p)	ON-center	$+1$
	OFF-center	-1

Table 2: Sign convention for the eye specificity and receptive field polarity variables describing functional properties of the RG and LGN cells.

processes and creation and destruction of synapses in the developing brain are surprisingly fast processes [1]. Competition and facilitation between RG cells to form and increase the strength of existing synapses on geniculate cells determine the outcome of the final pattern of connectivity.

The maturation of the retinogeniculate projections is the process of development of $s_{ij}(\tau)$ from the initial condition $s_{ij}(0) = 0$ for all i and j. The process of development of the various maps in the LGN, i.e., the establishment of layers, the retinotopic property of the maps and their strict registration, is a result of establishment of particular retino-geniculate connections. At any given time the values of $s_{ij}(\tau)$ completely determine the response of c_j given the activities of the RG cells, and, therefore, the values of $s_{ij}(\tau)$ determine the form and quality of the emerging maps.

In the mature state of the LGN, few RG cells connect to any given LGN cell and few LGN neurons receive input from a given RG cell. In addition to the "few-to-few" property of the mature mapping, all surviving LGN neurons receive input from the same type RG cells with extremely similar retinal coordinates. The mature LGN neurons receive pure input, as opposed to the initial nonexistent or mixed input of unmature LGN neurons.

Numerical values for the binary-valued parameters of the RG cells can be assigned as $+1$ or -1. Let contralateral RG cells have eye specificity $+1$, and the ipsilateral cells -1. Let cells with ON-center receptive field have $+1$ polarity, while the OFF-center ones have polarity -1. Table 2 summarizes the chosen convention.

One can now define cumulative variables describing LGN neuronal functional properties derived from the connections they have with the RG cells. These are the normalized LGN eye specificity and RF polarity, defined as the following weighted averages:

$$e_j^L(\tau) = \frac{\sum_{i=1}^{M} e_i\, s_{ij}(\tau)}{\sum_{i=1}^{M} s_{ij}(\tau)} \tag{1a}$$

$$p_j^L(\tau) = \frac{\sum_{i=1}^{M} p_i\, s_{ij}(\tau)}{\sum_{i=1}^{M} s_{ij}(\tau)}, \tag{1b}$$

where e_i and p_i are the numerical values assigned to the eye specificity and polarity of RG cell g_i. The above expression, of course, is meaningless if the sum of the synapses on c_i is zero. In this case, the values of $e_j^L(\tau)$ and $p_j^L(\tau)$ are set to zero.

The values of these integral and normalized variables describing the neuron c_j lie always between -1 and $+1$. A neuron with purely contralateral input will have $e_j^L = +1$. Similarly, purely OFF-center input will mean $p_j^L = +1$. A value of zero for these variables means either no input at all, or input from both types with equal strength. The above definition of geniculate eye specificity and polarity does not take into account the retinal position of the varying input RG cells.

Rigorous modeling of the development of the LGN cell functional properties requires one to keep track of all connections between all RG cells and all LGN neurons, i.e., one has to deal with an $M \times N$ matrix $\{s_{ij}\}$. This means that the computation would scale as $O(N^2)$, since $M \approx N$. In the numerical simulations presented later the number of modeled LGN cells is typically $N = 4800$. One needs at least several thousand cells in order to fill a 3-D body with reasonable cell density and a reasonable number of cells per projection column. (The macaque LGN contains about 1,000,000 cells.)A large number of LGN cells is also necessary in order to model the propagation of the wave of developmental as a smooth process. In fact, $N = 4800$ is about the minimum number that can be chosen safely, it translates into about $20 \times 12 \times 20$ cells along the dimensions of the LGN volume.

In addition to any retino-geniculate interactions, one has to consider internal LGN cell-cell interactions and the influence of any external morphogenetic gradients (which are necessary to account for the stereotypical ordering of the cell strata). Such a full-scale model is impossible to implement numerically. Hence, the integral variables for eye specificity and RF polarity of the LGN cells (defined in Eqs. (1a, 1b) are used as the variables subject to change during LGN development. Additional reasons for this choice is that

these variables are observable, they can and are measured in physiological experiments, and one knows that in their final, mature state the LGN cells have pure values of their compound eye specificity and polarity: $e_j^L, p_j^L = \pm 1$.

The establishment of the precise retinotopic nature of the retinogeniculate maps will not be modeled. It is assumed that the following factors strongly facilitate emergence of retinotopy: relatively slow propagation of the developmental wave from a small starting region (representation of the very central fovea), and the apparent faster development within projection columns. More discussion on this topic will be presented below.

The variables describing the functionality of the i-th LGN neuron (the eye specificity and receptive field polarity[6]) are real functions of a discrete time variable τ:

$$e_i(\tau),\ p_i(\tau)\ \in\ [-1,1]\ \subset\ \Re,\ i=1,2,\ldots,N,\ \tau=0,1,\ldots,T_{max}. \qquad (2)$$

According to the definition of these variables, Eqs. (1a,1b), their limiting values ± 1 correspond to the case when the i-th LGN neuron receives pure-type (eye specificity or polarity) input. The chosen convention for the signs of the cell functional properties was given in Table 2 above.

The initial condition is chosen as

$$e_i(0)\ =\ p_i(0)\ \equiv 0,\ i=1,2,\ldots,N, \qquad (3)$$

which, as explained before, could be a result of completely balanced input on all LGN cells, including $s_{ij}=0$ for all cells (no synapses between the RG and LGN cells).

The values of the eye specificity and polarity variables at time $\tau+1$ depend on their values at time τ, on the state of the nearby cells, on the position of the cell in the LGN, and on some stochastic contribution.

The full set of equations describing the dynamics of the cell variables $e_i(\tau)$ and $p_i(\tau)$, $i=1,\ldots,N$ is given by

$$\hat{e}_i(\tau+1)\ =\ e_i(\tau)+\Delta e_i(\tau)+\eta_e, \qquad (4a)$$

$$\hat{p}_i(\tau+1)\ =\ p_i(\tau)+\Delta p_i(\tau)+\eta_p, \qquad (4b)$$

[6]From now on we will omit the superscript "L" (for LGN) of eye specificity and polarity variables as defined in in Eqs. (1a, 1b).

$$\Delta e_i(\tau) = \alpha(r_i)\left(1 - e_i^2(\tau)\right)\beta_{ab}^t\left[\left(\sum_{j=1}^{N} e_j(\tau)\, f(|r_i - r_j|)\right) + E_{ext}(r_i)\right] \quad (5a)$$

$$\Delta p_i(\tau) = \alpha(r_i)\left(1 - p_i^2(\tau)\right)\beta_{ab}^t\left[\left(\sum_{j=1}^{N} p_j(\tau)\, f(|r_i - r_j|)\right) + P_{ext}(r_i)\right] \quad (5b)$$

$$e_i(\tau+1) = \min\left(|\,\hat{e}_i(\tau+1)\,|,\ |\hat{p}_i(\tau+1)\,|\right)\operatorname{sgn}\left(\hat{e}_i(\tau+1)\right), \quad (6a)$$

$$p_i(\tau+1) = \min\left(|\,\hat{e}_i(\tau+1)\,|,\ |\hat{p}_i(\tau+1)\,|\right)\operatorname{sgn}\left(\hat{p}_i(\tau+1)\right). \quad (6b)$$

A discussion of the particular choice of functional dependencies and the interpretation of the various parameters and terms follows.

Since eye specificity and RF polarity variables enter symmetrically in the dynamics, we will address only the interpretation of the equations for eye specificity development. All that will be said about the dynamics of eye specificity is readily translated to the dynamics of RF polarity variable.

On the left hand-side of Eq. (4a) an intermediate variable $\hat{e}_i(\tau+1)$ is introduced. This is a virtual variable, an intermediate step towards determining the value of $e_i(\tau+1)$. $\hat{e}_i$ is a non-observable. It is a sum of three terms: the value of e_i at the previous time step, a deterministic change and a stochastic change. Through the virtual variables for eye specificity and polarity, $\hat{e}_i$ and $\hat{p}_i$, a coupling between cell development within a projection column is accomplished [Eqs. (6)].

The stochastic term η_e incorporates a degree of randomness in the growth and retraction of the retinogeniculate synapses. This developmental noise plays an important role in allowing the system to explore larger areas of its state space (formation of cell clustering) and plays a driving role for the switch of the state at the position of the optic disk gaps. The values of η_e are drawn from a uniform distribution in an interval $[-\eta_{max}, +\eta_{max}]$. The limiting values of this interval are the same for both eye specificity and polarity variables.

The deterministic change $\Delta e_i(\tau)$ is calculated according to Eq. (5a). The value of $\Delta e_i(\tau)$ depends on the influence of the neighboring cells, i.e., on their own developmental state, on the location of the cell in the LGN, and on its own susceptibility to change. Equation (5a) can be written in the form

$$\Delta e_i(\tau) = S_i(\tau)\, E_i^{tot}(\tau), \quad (7)$$

where $S_i(\tau)$ is the susceptibility at time τ of the i-th neuron to change its eye specificity, and $E_i^{tot}(\tau)$ is the current total field, acting to change the neuron's eye specificity. The cell susceptibility is given by

$$S_i(\tau) = \alpha(r_i)\left(1 - e_i^2(\tau)\right)\beta_{ab}^t, \tag{8}$$

and the total field by

$$E_i^{tot}(\tau) = \left(\sum_{j=1}^{N} e_j(\tau) f(|r_i - r_j|)\right) + E_{ext}(r_i). \tag{9}$$

The cell susceptibility for the eye and polarity variables is the same at all times (this will become clear below), while the total eye and polarity fields may be different. In this view, the neuronal variables are subject to a total field felt by the neurons. A stronger field will yield larger changes in the variables. For example, if a positive eye specificity field is acting on a neuron, and its susceptibility is positive, the effect of the field will be to increase the value of $e(\tau)$, and so increase the eye preference towards the contralateral eye. The effect of the field is modified by the internal neuronal susceptibility to change. The susceptibility depends on the developmental state, location, etc. of the neuron. It is always non-negative, while the total field can have either sign. A non-zero susceptibility means that the neuronal variables change following the direction of the acting field, never going opposite to its action[7].

The total eye specificity field acting on the i-th neuron (which is located at r_i) has two components:

$$E_i^{tot}(\tau) = E_{int}(r_i, \tau) + E_{ext}(r_i). \tag{10}$$

The internal field $E_{int}(r_i, \tau)$ is created by the surrounding cells; it depends on their own state, and, therefore, is time-dependent. The external field $E_{ext}(r_i)$ is an expression of morphogenetic gradients which do not depend on the state of the LGN cells and are probably created by structures external to the LGN. In principle, the external field can be time-dependent (most likely

[7]When the cells are in their mature state $e_i \approx \pm 1$, small fluctuations due to the noise may cause negative susceptibility. This state lasts, however, a very short time.

in the real system it is slowly changing in time), but in our model it does not depend on time[8].

The internal (or cell) field embodies the action of the possible by which LGN neurons may interact and influence each other's development. The form of the internal field is

$$E_{int}(r_i, \tau) = \sum_{j=1}^{N} e_j(\tau) f(|r_i - r_j|). \tag{11}$$

This equation is interpreted as follows: the internal field acting on neuron c_i, at position r_i, is a linear superposition of the fields created by its neighboring neurons. The contribution of neuron c_j is proportional to the degree of its own development, i.e., to $e_j(\tau)$, and to some interaction function $f(|r_i - r_j|)$ of the distance, $|r_i - r_j|$, between the neurons c_i and c_j. The interaction function f describes the magnitude of neuronal interaction as a function of the distance between the two cells. A Gaussian, with characteristic distance σ, is chosen for the interaction function

$$f(\delta) = \exp(-\delta^2/\sigma^2). \tag{12}$$

The range of the interaction mechanisms is approximated by the value of σ. The value of σ could be interpreted as the size of the RG-cell axonal arborization or, alternatively, the characteristic diffusion range of the neurochemicals responsible for the presumed neuronal interactions. The value of σ could also be related to the size of the dendritic trees of the LGN cells, since close-range dendritic interactions are another possible underlying mechanism for the neuronal interactions during development.

Any external morphogenetic gradients influencing cell development are incorporated in the term $E_{ext}(r_i)$ for the external field. The necessity to include an external field in the model follows from the observation that the ordering of the LGN layers in the dorso-ventral (top-to-bottom in the head) axis is always 6-5-4-3-2-1 in the central vision region. In the cat, the different arrival times of the contralateral and ipsilateral projections have been suggested as an explanation of the fixed ordering of the LGN layers[39]. In macaque, however, the RG cell axons from both eyes arrive simultaneously.

[8] Any choice of a time dependence of the external field would have introduced additional parameters in the model and most likely would be based on pure speculations.

Besides, in macaque, there is the additional complicating rule that ON-center cells form layers on top of the OFF-center cellular layers (Figure 3). Hence, there must be an externally derived reason which causes always the same ordering of the layers.

The external field plays two roles: 1) it stabilizes (and thus effectively determines and launches) a particular laminar configuration of the system in the foveal part of the LGN. 2) it shapes (or simply promotes without enforcing) a particular peripheral lamination pattern. Accordingly, it is convenient to consider it as consisting of two terms:

$$E_{ext}(r_i) \;=\; E^f_{ext}(r_i) + E^p_{ext}(r_i). \tag{13}$$

The first term $E^f_{ext}(r_i)$ is dominant in the foveal LGN, while the second term $E^p_{ext}(r_i)$ dominates in the peripheral LGN. Furthermore, it is assumed that the magnitudes of the foveal and peripheral contributions, correspondingly, decrease and increase, from the foveal to the peripheral LGN representations. We will use the names "foveal and peripheral external fields" for the two terms in Eq. 13. The foveal and peripheral external fields have different forms and promote different lamination patterns. The mature state of the LGN results from the competition between these two fields, as well as, from the tendency of the system to remain in a homogeneous state due to the cell interactions (the internal field promotes homogeneity of the lamination across the LGN).

The form of the foveal fields for the eye specificity and the polarity is:

$$\begin{aligned} E^f_{ext}(x,y,z) \;&= A_f \,\exp(-x)\,\times \\ &\quad \times\left[\,\theta(z-d) - 2\,\theta(z-2d) + 2\,\theta(z-3d) - \theta(d-z)\,\right] \qquad (14a) \\ P^f_{ext}(x,y,z) \;&= A_f \,\exp(-x)\,\left[\,2\,\theta(z-2d) - 1\,\right], \qquad (14b) \end{aligned}$$

where, $d = S_z/4$ is the thickness of a layer in the F lamination pattern, and the "theta" function is defined, as usual, as $\theta(x) = 1, x > 0$ and $\theta(x) = 0, x < 0$. The value of the factor A_f in both expressions sets the magnitude of these fields. Note that both of them decay very quickly as one moves away from the foveal representation ($x = 0$). The shapes of the fields along the z axis are chosen such that they directly promote development of eye and polarity variables in concert with the final ordering of cell strata found in the foveal (F) pattern.

The form of the peripheral fields used to promote the P pattern is

$$E^p_{ext}(x,y,z) = A_p\,[\,2\,\theta\,(z-2d)-1\,] \tag{15a}$$

$$P^p_{ext}(x,y,z) = A_p\,[\,\theta\,(z-d)-2\,\theta\,(z-2d)+2\,\theta\,(z-3d)-\theta\,(d-z)\,] \tag{15b}$$

These fields do not depend on x, i.e., they are present in the whole length of the LGN. The foveal external fields, on the other hand, are restricted only to the foveal representation due to the factor $\exp(-x)$ in Eq. (14). The magnitude of the peripheral fields is set by the factor A_p. The graphs of all four external fields as functions of the z-coordinate are presented in Figure 5.

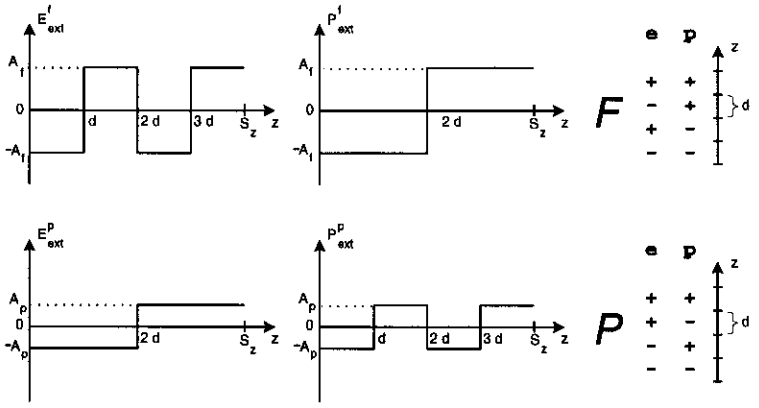

Figure 5: The form of the foveal (top) and peripheral (bottom) external fields as a function of the z coordinate. The fields acting on the eye specificity variable are in the left column, the ones acting on the polarity variable are in the middle column. The right column presents the signs of the eye and polarity variables of a projection column in the F and P pattern. The signs of all fields are such that the fields directly promote one or the other pattern. The thickness of a cell stratum is $d = S_z/4$.

The step-like forms of the external fields, Eqs. (14 and 15), are biologically unrealistic. Any morphogenetic gradients in a developing LGN are likely to be continuous monotonic functions of the spatial coordinates. In the Appendix we show how such monotonic gradients can be employed to influence development within one projection column and to lead to a particular ordering of cell strata. However, continuous and monotonic forms of the gradients require a more microscopic level of description of the system, i.e., require one to keep track of individual synapses between RG and LGN

cells. On the present mesoscopic level of description of the cells one can work with fields acting directly on the eye specificity, $e_i(\tau)$, and RF polarity, $p_i(\tau)$, variables, which are composite quantities [Eq. (1)]. Therefore, the external fields at this level are also composite quantities and do not have necessarily all of the properties of microscopic morphogenetic gradients.

The foveal external fields dominate in the foveal region (near $x = 0$), which requires $A_f > A_p$. The foveal fields decay exponentially with x in such a way that the peripheral fields dominate in the periphery. It is obvious from the expressions for the external fields, Eqs. (14, 15), that at some crossover eccentricity x_c the magnitudes of the two types of fields will be equal. The value of x_c is determined by the condition

$$A_f \exp(-x_c) = A_p, \tag{16}$$

which leads to

$$x_c = \ln \frac{A_f}{A_p}. \tag{17}$$

Let's now return to the susceptibility factor in Eq. (7) given by Eq. (8) The factor $\alpha(r_i)$ describes the susceptibility, or the rate of change of the cell variables, and is the same for eye specificity and polarity variables. This factor depends on the position r_i of the cell to account for spatially non-uniform development (to partially compensate for the fact that the model LGN is flat, while the real LGN is not, and to account for the inhomogeneity of the density of the retinal input[9]). The functional dependance is chosen as $\alpha(x, y, z) = \alpha_0 (0.1 + \exp(-(y - S_y/2)^2))$, attributing higher susceptibilities to cells along the horizontal meridian.

The second multiplicative factor in Eq. (8) provides a feedback mechanism for cell development: the more mature a cell is (e_i closer to $+1$ or -1), the less susceptible it is to change. In this way one can incorporate the gradual loss of plasticity of the LGN neurons. Most likely this loss is regulated by external factors in the real system, which, for the sake of simplicity, are not included in the model. The nonlinear term in Eq. (8) incorporates the loss of plasticity while also ensuring that ± 1 are the only stable fixed points of the dynamics. For most of the neurons, the eye specificity and polarity variables gradually converge to either of these fixed points, or, equivalently, the cells acquire

[9]The density of RG cells on the horizontal meridian is larger than on other meridians, for the same eccentricity[27].

The four types of LGN cells and the signs of their variables			
		eye specificity (e)	
		+ (CONTRA)	− (IPSI)
center polarity (p)	+ (ON)	6	5
	− (OFF)	4	3

Table 3: The four types of parvocellular LGN cells and the signs of their variables.

pure functional properties, which are a manifestation of cell maturity. Some small portion of the cells will remain in an undetermined state ($|e_i, p_i| < 1$). Such cells tend to concentrate on the borders between the forming layers. The nonlinearity stabilizes the dynamics, preventing divergence of the cell variables.

The third term in Eq. (8) is related to the remarkably strict columnar organization of the visual-space representation in the LGN. Even when cells are not completely mature, they are referred to as being of four different types, depending on the signs of their functional properties, as shown in Table 3.

Development of the LGN appears to possess two inherent time scales. The first one is related to lamination within projection columns, the second to the spread of lamination from column to column. Development within a column has a much shorter time scale than the time scale of the propagation of the wave from one edge of the LGN to the other. Development of the projection columns as individual objects is incorporated by imposing the restriction that all four types of LGN cells (defined by the input they receive) emerge and remain in approximately equal numbers in any given column. This restriction is also related to the fact that four types of RG cells exist in about equal numbers in the homologous coordinates of the retinas and must make connections to their respective column in the LGN. These observations are taken into account by the third factor $\beta^t_{ab}(\tau)$ in the right-hand side of Eq. (8). At each step of the development the proportion of all four types of LGN cells is calculated within a single column C_{ab}, and $\beta^t_{ab}(\tau)$ for different types t is adjusted such that all types remain equally represented in the column. For over-represented cell types $\beta^t_{ab}(\tau) < 1$ holds; for under-represented

cell types $\beta_{ab}^t(\tau) > 1$ holds. In this way one achieves a balanced growth of all types of functionalities. Without this term, the cell developmental pattern degenerates to a non-laminar one; the system tries to minimize the boundaries between clusters of different-type cells and evolves to a collection of oval-shaped clusters.

$\beta_{ab}^t(\tau)$ is calculated in the following way: at any given time τ, within the column C_{ab}, the number $N_{ab}^t(\tau)$ of cells, that could be classified as one of the four types $t = 3, 4, 5, 6$, is counted. Cells with $e_i(\tau)$ or $p_i(\tau)$ exactly zero are not counted. The total number of classified cells is then $N_{ab}(\tau) = \sum_{t=3}^{6} N_{ab}^t(\tau)$. If there are no classified cells ($N_{ab}(\tau) = 0$), then $\beta_{ab}^t(\tau)$ is set to one for all t. Otherwise the ratio of different types is calculated: $n_{ab}^t = N_{ab}^t(\tau)/N_{ab}(\tau)$. Finally, $\beta_{ab}^t(\tau)$ is calculated using

$$\beta_{ab}^t(\tau) \;=\; 4 - 12\, n_{ab},\; t = 3, 4, 5, 6. \tag{18}$$

If $\beta_{ab}^t(\tau)$ so calculated is negative, it is replaced by zero. The really important properties of the function $\beta = \beta(n)$ are that $\beta(1/4) = 1$ holds, and that $d\beta/dn < 0$, at $n = 1/4$ holds. The larger the absolute value of $d\beta/dn$ at $n = 1/4$, the stronger is the negative feedback in a column and the more strictly enforced is the equal representation of four cell types.

After the values of the intermediate variables, $\hat{e}_i(\tau)$, are calculated, Eq. (6a) is used to find the values of the observables, $e_i(\tau + 1)$, at the next time step. The form of Eqs. (6a, 6b) forces the cells to remain, for all times, in a state in which $|e_i(\tau)| = |p_i(\tau)|$. This constraint, combined with the change of susceptibility of the cells governed by the β term, ensures that the amount of input from the four types of RG cells is balanced in any column. This somewhat intricate procedure is required since establishment of retinotopy and columnar organization is not modelled from more basic principles, which could give automatically equal representation of all types of RG input in a column.

The model separates the time scales in the LGN development, assuming that fast developmental processes ensure the right structure of the projection columns. What is really modeled is the slower process – the propagation of the lamination pattern from column to column, and therefore through the LGN.

The presence of the optic disk gaps in the LGN is due to the lack of corresponding RG cells in the optic disk in the contralateral hemiretina.

Accordingly, the blind spot gaps are modelled by imposing, at all times, a restriction $e_i(\tau) \geq 0$ on the allowed values of the eye specificity of the cells in certain projection columns. Consequently, some cells in these columns never reach a pure state characterized by $e_i, p_i = \pm 1$. It is assumed that in reality cells that fail to reach a pure state die out. Elimination of such cells eventually produces the optic disk gaps and helps delineate the LGN layers.

The size g of the optic disk gaps, assumed to be of square shape, is a parameter of the model. Another important parameter is the range of cell-to-cell interactions, σ. It turns out that the density of cells and the interaction range determine the magnitude of the internal field. The latter field depends also on the emerging clustering pattern. The ratio between the magnitude of the internal and the external field (which may promote a lamination pattern different from the current one), as well as the magnitude of the noise in the dynamics determine the stability of the current laminar pattern.

It should be pointed out that only the variables describing the functional properties of the LGN neurons depend explicitly on time. All other variables derive their time-dependence through $e_i(\tau)$ and $p_i(\tau)$.

3 Numerical Simulations

In this section are presented results of numerical simulations of the full model. The stability of propagation of the developmental wave and its interaction with the optic disk gaps is studied in two and three dimensions for various external fields, cell densities and interaction distances, as well as, different gap sizes and locations.

The simulations discussed below are numbered with roman numerals; the values of the parameters used in the simulations and some comments about the simulations are given in Table 4. The first column of this table contains the simulation number. Columns 2 through 7 contain the values of the corresponding parameters. The entry in column 8 indicates whether the projection column structure has been enforced in the simulation (see below for details). The last column contains the labels of the figures in which the results of the simulations are shown.

the figure numbers have to be adjusted

Some parameters have the same values in all simulations discussed below. These parameters include $\sigma = 1.0$, $S_x = 10$, $S_z = 6$, $\eta_{max} = 0.002$, $\alpha_0 = 0.0001$.

1	2	3	4	5	6	7	8	9
Simulation #	S_y	ρ	A_f	A_p	x_g	g	proj. col.	figures
I	0	44	100	0	–	–	no	6.A,B,C
II	0	44	100	50	–	–	yes	7.A,B,C
III	0	25	100	0	4	1.0	yes	9.A,B,C
IV	0	25	100	0	4	1.3	yes	9.D,E,F
V	0	25	100	50	3	1.0	yes	10.A,B,C
VI	0	25	100	50	3	1.0	yes	10.D,E,F
VII	10	8	10	5	–	–	yes	12.A,B,C,D
$VIII$	10	8	10	5	4	1.0	yes	13.A,B,C,D
IX	10	8	100	70	4	1.0	yes	14.A,B,C,D

Table 4: Values of the parameters in various simulations discussed in the text. The cell density ρ, column 4, is given in units of #cells/length^2 for the two-dimensional models ($S_y = 0$), and in units of #cells/length^3 for the three-dimensional models ($S_y \neq 0$). In all simulations the foveal fields decay as $\exp(-x)$; the only exception is Simulation VI in which the foveal fields decay as $\exp(-x/2)$. The sign "–" is used when the corresponding parameter is not applicable.

3.1.1 The Role of the Projection Columns

Enforcement of projection columns is crucial for stable propagation of any pattern in which cells of different types are present and lie in neighboring layers. Without this constraint the LGN structure degenerates to one that contains only one type of cells. It was shown in the previous Chapter that the boundaries between clusters of cells of different types carry most of the energy. Therefore, one expects that if equal numbers of cell of different types are not enforced (locally or globally in the system), a layered pattern of cell organization will not be stable. The system tries to minimize the boundaries between clusters which should lead to development of only one cell type, i.e., to no cluster boundaries at all.

Simulation *I* illustrates development of a two-dimensional system in which the projection column structure is not enforced[10]. The dynamics used is described by Eqs. (4, 5, and 6); the β_{ab}^{t} factor in Eq. (5) is set to unity for all cell types, t. In other words, all cell types compete freely throughout the entire system. Figure 6 shows three stages of development. The F pattern (with ordering of the strata 6, 5, 4, 3 along the z axis) is started at $x = 0$ (Figure 6.A) by external fields with only the foveal components, Eq. (14). There are no peripheral fields. The system develops on its own far from $x = 0$ because the foveal fields decay quickly along the x axis. Cells are represented as circles with different shades depending on the cell type. As time progresses, more and more cells acquire functional properties, and the developmental wave spreads in the undeveloped part of the LGN. The laminar pattern of the LGN, however, changes with x. First layer 4 is squeezed out (Figure 6.B), then layer 5 (Figure 6.C). Eventually, for large x, only one cell type remains. Usually, this is one of the outer layers (6 or 3) because they are subjected to competition from only one side (the inside of the nucleus), while the middle layers have to compete for space from both (upper and lower) sides. One can also see that some cells in the interface between layers fail to develop terminal functionalities. In this way, they help to delineate the borders between the cell layers.

The degree of instability of the laminar pattern depends on the interaction

[10]Here and when other simulations are discusses, the reader is referred to Table 4 for the values of the parameters.

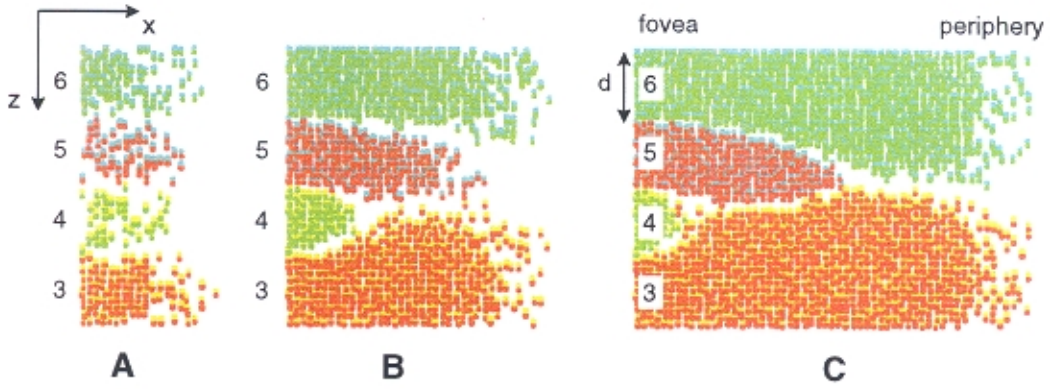

Figure 6: Development of a two-dimensional system without enforcement of equal cell type representation within projection columns (Simulation *I*). Developing LGN cells are represented as shaded circles. The different shades represent different cell types. Each cell is classified as being of a particular type if the absolute values of the eye specificity and RF polarity variables are larger than 0.1. Undeveloped or little developed cells, with absolute values of e_i and p_i less than 0.1 are not drawn. The system is shown at three consecutive moments. **A**: Development is started near $x = 0$ in a laminar pattern with all four types of cells present. **B**: Lamination progresses to the right but is unstable: layers 5 and 3 take over the space of layer 4 and terminate its propagation. **C**: The middle layers are eliminated because they face constant competition from both sides.

distance, σ, and on the thickness, d, of the layers near the fovea. The larger the ratio σ/d is, the more unstable the pattern. For $\sigma/d \geq 1$ all cells in a layer "feel" the fields created by cells in neighboring layers in addition to the fields of nearby (usually same type) cells within their own layer. The total local fields are not very strong because the fields created by different type cells cancel each other. The developmental process is more susceptible to fluctuations, and can be disrupted more easily. When σ/d is small, only cells near the border of a layer feel the fields of cells in neighboring layers. The majority of the cells, in the middle of any layer, are subjected to fields, created mostly by cells of the same type. These middle-layer cells develop in synchrony, acquiring the same functional properties, and making the laminar structure more stable.

The purpose of Simulation *II* is to show how enforcement of the columnar organization stabilizes the laminar pattern. In this simulation the β^t_{ab} factor in Eq. (5) is a function (as described on page 22) of the cell type, t. Fig-

ure 7 illustrates results of the simulation. The seed F pattern (Figure 7.A) is started by localized foveal fields, Eq. (14), with $A_f = 10$. These fields are present only in the foveal part of the nucleus, $x \approx 0$, and are virtually zero everywhere else. Peripheral external fields, Eq. (15) with $A_p = 5$, oppose the propagation of the F pattern, and favor the P pattern of strata ordering. However, the internal fields created by mature cells and the projection-column constraint stabilize the F pattern, and cause it to spread through the whole nucleus (Figure 7.B and Figure 7.C).

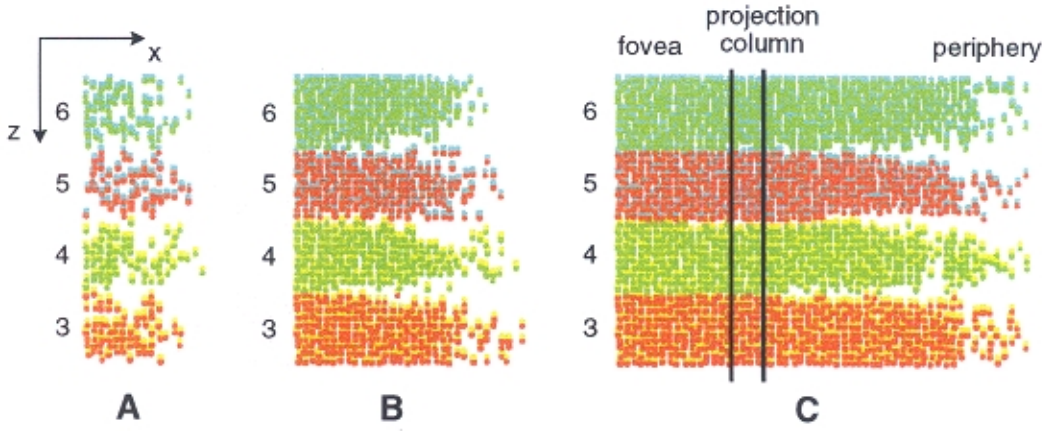

Figure 7: Development in a two-dimensional system with enforcement of projection columns and peripheral fields (Simulation II). As in Figure 6, the system is shown at three consecutive moments. **A**: Development is started near $x = 0$ in a laminar pattern with all four types of cells present. **B**: Development progresses to the right. **C**: The four-layer structure is preserved despite the presence of peripheral fields which favor cell strata rearrangement. The numbers of cells of the four types in projection columns are kept in equal proportion by the underlying dynamics.

Simulation II provides an example of a propagation of a metastable state through the whole system. Obviously, for large x, the P pattern has lower energy than the F pattern. However, there is an energy barrier that the system must overcome in order to switch F to P state. Stability of the F state is additionally increased by strict enforcement of the projection column organization. In fact, without enforcement of this organization laminar patterns cannot propagate through the nucleus.

3.1.2 Velocity of Propagation

In [43] an expression for the propagation velocity of the wave of development in a two-dimensional nucleus is calculated:

$$v_{min}^{(2)} = \sqrt{\frac{e}{2}}\,\pi\,\alpha\,\rho\,\sigma^3 \approx 3.663\,\alpha\,\rho\,\sigma^3. \tag{19}$$

where α is the rate of cell development, λ is the cell density and σ is the interaction distance. This expression is obtained for a non-laminated nucleus.

.

need to add a line for d - infty, no lamination

Figure 8 shows the measured velocity of propagation of the F pattern as a function of the interaction distance, σ, and the layer thickness, d. For small values of σ/d, the measured values of v agree very well with the predictions for a two-dimensional traveling wave, given by Eq. (19). In this limit, only a small fraction of the cells in each layer feel the presence of cells of different type in other layers. This leads to an almost independent development of each layer. The projection column constraint ensures the preservation of laminar order (and keeps the laminar interfaces relatively straight) but has little effect on the velocity of propagation.

For $\sigma/d \geq 0.4$ Eq. (19) does not correctly predict the measured velocity. Simulations produce smaller than predicted values. At this point the presence of the layer boundaries becomes significant. Layers cannot be treated as developing independently from one another. Consider a given layer (let it be labeled layer A). The fields created by cells from neighboring layers have a braking effect on the propagation of A. The reason is that the sign of at least one functional property differs between the cells of any two layers. This effect becomes more and more pronounced as σ/d increases. At some value of this ratio the velocity of propagation peaks, as illustrated by the graph for $d = 1.0$ of Figure 8. Beyond this point, an increase of σ leads to a decrease of v. This is due to the increasingly larger time needed to ensure preservation of the laminar pattern. Layers invade other layers' bands too "aggressively", and more time is needed for the projection column mechanism to correct such mistakes.

If disk gaps are present in the system, the incoming wave of development will interact with them. Depending on the parameters of the system (cell density,

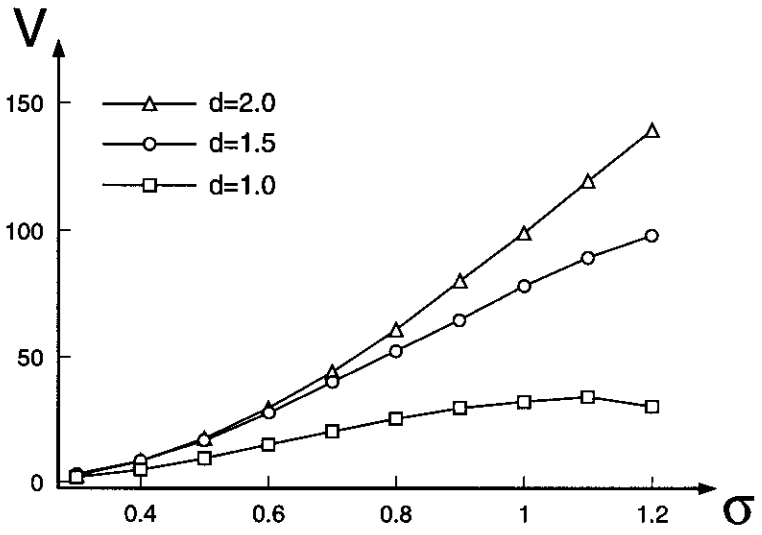

Figure 8:
Velocity of propagation of the F pattern as a function of the interaction distance σ. Plots for three values of the layer thickness, d. The values of the velocities are normalized for different cell densities. For $\sigma/d < 0.4$ the velocity is very well predicted by Eq. (19). For larger values of this ratio the measured velocity is less than the theoretical one.

interaction distance, gap size, layer thickness, magnitude of the peripheral fields, etc.) several outcomes of this wave-gap interaction are possible. The cell density, ρ, and the interaction distance, σ, determine the magnitude of the internal fields[11] (the fields created by cells which have already reached some degree of maturity and have nonzero values of e_i and p_i). The stronger the internal fields are, the more stable is the propagation of the F pattern. The size of the gaps, g, is a measure of the magnitude of the perturbation induced by the gaps. The larger g is, the easier an incoming F pattern can

[11] In a two-dimensional system the internal fields depend on the degree of development, as well as on the laminar pattern, and are proportional to $\rho\sigma^2$. For example, in a fully developed homogeneous system the local eye-specificity or polarity fields are given by the same expression, $\int_0^\infty 2\pi\rho \exp(-r^2/\sigma^2) = \pi\rho\sigma^2$; both fields do not depend on r and are proportional to $\rho\sigma^2$.

be abandoned for a more stable one[12].

Results of Simulations III and IV illustrate the role of gap size. These two simulations differ only in the value of the gap size; in Simulation III the gap size is $g = 1.0$, in Simulation IV it is $g = 1.3$. Figure 9 contains results of the two simulations. The left column displays the state of the LGN during Simulation III, the right column displays the state of nucleus during Simulation IV. Pictures on the same horizontal level in Figure 9 present the state of the system in the two simulations at the same times.

Figure 9.A shows the system in Simulation III; the incoming F state has just jumped the gaps. Figure 9.D shows the system in Simulation IV at the same time as in Figure 9.A; the incoming F pattern has reached the gaps but is not able to continue past them unchanged because layers 5 and 3 have grown into the gap of layer 4 and have stopped its growth. Development takes different routes because in Simulation IV the gaps are wide enough and allow layers 5 and 3 to establish firm presence and link in the gap of layer 4, while in Simulation III, with narrower gaps, layers 5 and 3 cannot link in the layer 4 gap. Figure 9.B and Figure 9.C show further development in Simulation III. The propagation of the F pattern continues beyond the gaps. Note the slight bulges of layers 5 and 3 at the gaps of layers 6 and 4. These bulges are remnants of the unsuccessful attempt of layers 5 and 3 to occupy the gap spaces. Figure 9.E and Figure 9.F show further development in Simulation IV. In Figure 9.E a new reordering of the cell strata is seen to the right of the gaps. Propagation of layer 4 has been stopped but the projection column constraint requires that all cell types be equally represented in the columns beyond the gaps. Cells of type 4 reappear beyond the gaps, not between cells of types 5 and 3 as in pattern F, but below cells of type 3. The new vertical position of the restarted layer 4 leads to a new laminar pattern. The new pattern is of X-type; it has a lower energy than the F pattern. Figure 9.D illustrates that once the new X pattern is established it propagates to the right and reaches the end of the LGN.

In Simulation IV the gaps induce the laminar transition. The particular order of the layers in the second laminar pattern may differ in simulations even with the same parameter values. For example, another frequently observed X-type pattern has top-to-bottom layer ordering 4, 6, 5, 3.

[12]Relative magnitude of the gaps' perturbation depends also on d and σ. Larger values of these parameters reduce the gaps' influence.

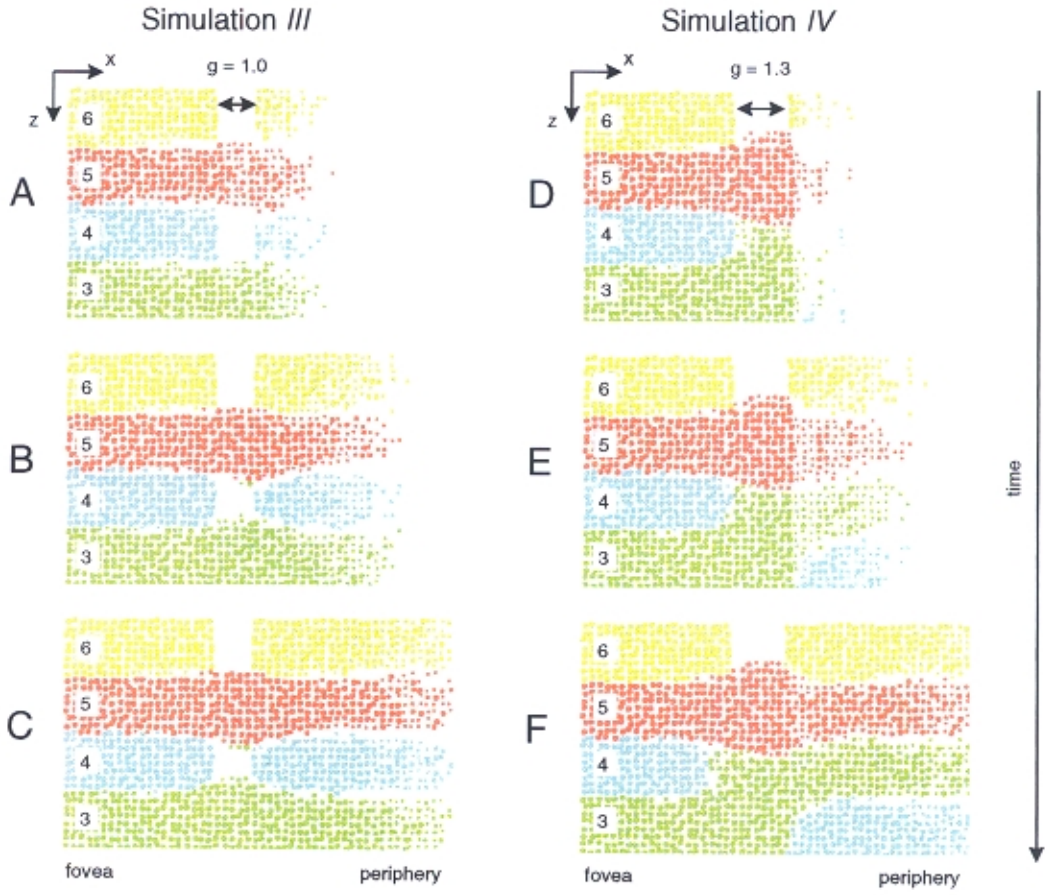

Figure 9:
Left column: three consecutive snapshots of the system in Simulation *III*. Right column: snapshots of the system in Simulation *IV*. The snapshots on the same horizontal level are taken at the same times. **A**: An F state, started in the foveal representation, propagates to the right towards the peripheral representation. The small size of the gaps allows the same pattern to be propagated beyond the gaps, $x > x_g + g$. Although in the gaps there are no cells of type 6 or 4, the field created by cells foveal to the gaps ($x < x_g$) is strong enough to start layers 6 and 4 peripheral to the gaps ($x > x_g + g$) at the same z level. **B** and **C**: The F state is further developing into the peripheral LGN. Note how layers 5 and 3 expand inside the gaps. **D**: Wider gaps allow layers 5 and 3 to expand more, filling the void of layer 4. This shields the field of layer 4 cells and prevents cells on the same level peripheral to the gaps from acquiring this type of functionality. **E**: Cells of type 4 reappear peripheral to the gaps at the bottom of the system. **F** This new X-type pattern is stable and is propagated peripherally. In both simulations the left edge of the gaps is at $x_g = 4$, there are no peripheral fields, layer thickness is $d = 1.5$, interaction distance is $\sigma = 1.0$, the cell density is $\rho = 25\,\text{unit}^{-2}$, and the magnitude of the foveal fields is $A_f = 100$.

If the cell density or the interaction distance are increased in Simulation IV, the internal fields created by cells of layer 4 will become stronger, and the F pattern may be able to propagate past the gaps for $g \geq 1.3$. Increasing layer thickness will also help the F pattern to pass the gaps because layers 5 and 3 will need more time to fill in the the gap in layer 4. This delay will allow layer 4 cells to the left of the gap to "project" their influence to the right of the gaps for longer times, which will lead to an increase in the likelihood that cells beyond the gaps will acquire type 4 properties at the same z level. This translates into an increased stability of the F pattern against the perturbative influence of the gaps.

When the gaps are wide enough to induce a laminar pattern transition, the pattern peripheral to the gaps is chosen according to the minimum energy principle. For this reason a lack of peripheral fields leads to peripheral patterns of X type (in which there is a minimum number of changes of the signs of functional properties of the cells in neighboring layers). If, however, peripheral fields are present, the lowest energy state of the system may be changed, and the gaps will induce a transition to this state.

Simulations V and VI are examples of developmental scenarios of a system with peripheral fields favoring the P pattern of layer ordering. The two simulations differ only in the way the foveal fields decay as a function of x; in Simulation V this dependence is $\exp(-x)$; in Simulation VI it is $\exp(-x/2)$. In both simulations the values of the parameters used are[13]: $g = 1$, $x_g = 3$, $d = 1.5$, $\sigma = 1.0$, $\rho = 25\,\text{unit}^{-2}$, $A_f = 100$, and $A_p = 50$. The two simulations have different locations of the crossover point x_c, where the peripheral and the foveal fields have equal magnitudes; in Simulation V this point is at $x_c \approx 0.7$, in Simulation VI it is at $x_c \approx 1.4$. For $x < x_c$ the foveal fields are stronger, and the F pattern has lower energy than the P pattern.

Results of the two simulations are shown in Figure 10 . In the left column are shown three consecutive snapshots of Simulation V; in the right column are shown snapshots at the same times of Simulation VI. Figure 10.A shows the F pattern, started near the origin, reaching the gaps. Note that at the position of the gaps, $x_g = 3$, the F state is already metastable since $x_g > x_c$. The gaps produce a large enough perturbation to induce a switch from the metastable F state to the more stable P state. Once established, the P

[13]The gaps are shifted to the foveal direction relative to the previous simulations in order to allow more space peripheral to the gaps where more transitions may occur.

pattern propagates to the right of the gaps, as shown in Figure 10.B and Figure 10.C. As expected, the propagation of this pattern is faster than the propagation of the F pattern.

The nature of the transition is illustrated in Figure 10.A. When the wave passes through the gaps, different cell layers behave differently. Layers 5 and 3 are not forbidden to grow inside the gaps, so they continue along the x axis. Moreover, because they do not experience competition from layers 6 and 4, layers 5 and 3 "infringe" on the territory of layers 6 and 4 along the z axis. At some point in the gap of layer 4, layers 5 and 3 meet, which leads to a further isolation of layer 4 to the left of its gap. On the other hand, layer 5 does not reach the lateral edge of the system ($z = 0$) and cannot inhibit sufficiently propagation of layer 6. Layer 6 is able to establish a larger foothold to the right of its gap at the same z level. Cells of type 4 appear in two clusters to the right of the gaps. The lower cluster is a result of some remaining influence of layer 4 to the left of the gaps; the upper cluster is a result of the peripheral fields, and of the fact that layer 4 could not develop as fast as other layers in this projection column. Once layer 4 is split in this way, its upper part can grow much faster than its lower part (because of the peripheral fields and because the lower part is still being squeezed by layers 5 and 3). In Figure 10.B and 10.C one sees how the lower cluster of type 4 cells to the right of the gaps gradually disappears, while the front of the developmental wave is completely in state P . Eventually this lower cluster disappears. In summary, the gaps allow layers 5 and 3 to stop layer 4. This layer reappears at a position consistent with the P pattern because of the peripheral fields. The P pattern propagates further into the undeveloped part of the LGN. If the peripheral fields were stronger, layer 4 would reappear beyond the gaps only at one location, next to layer 6, and there would be no (even temporary) laminar pattern hesitation.

Simulation V illustrates how the gaps can trigger a transition to a favored non-X pattern. Simulation VI illustrates another scenario in which the F pattern propagates through the gaps, but a transition to the P pattern occurs at a more peripheral location. The crossover point is at $x_c = 1.4$ and the foveal fields are non-negligible at the location of the gaps, $x_g = 3$. In this case the gaps exert too weak a perturbation, and the F pattern passes through them unaltered as shown in Figure 10.D.

At some more peripheral point ($x \approx 6.5$), however, a spontaneous transition between the F and the P patterns occurs. The transition is shown

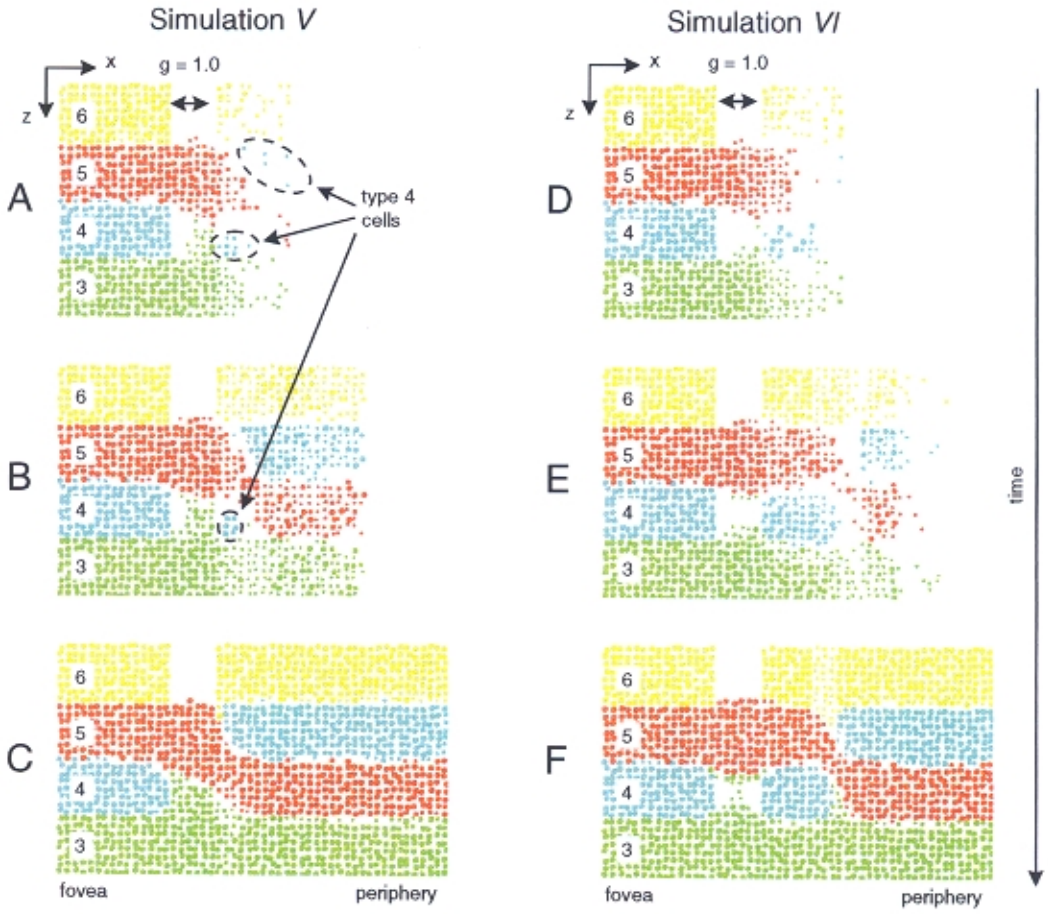

Figure 10:
Left column: results of Simulation V; right column: results of Simulation VI which has more slowly decaying foveal fields than Simulation V. The snapshots on the same horizontal level are taken in the same times. **A**: An F pattern started in the foveal representation has reached the gaps. Layers 6, 5 and 3 jump the gaps; cells of type 4 also appear peripheral to the gaps but in two discontinuous clusters. **B**: The upper cluster of type 4 cells has established a new vertical position of layer 4, leading to a new laminar pattern, consistent with the peripheral fields. **C**: The new P pattern is established in the entire peripheral part of the system. The lower type 4 cell cluster has disappeared. **D**: More slowly decaying foveal fields allow an incoming F pattern to jump successfully the gaps. **E**: At some point, $x \approx 6.5$, the foveal and internal fields cannot compensate the strong peripheral fields and the lamination switches to the P pattern. **F**: The P pattern reaches the peripheral end on the system.

in Figure 10.E. At the transition point the support of the foveal fields has dropped too much and the F pattern is not a sufficiently stable state of the system. Fluctuations in the development bring the system over the energy barrier to another deeper state (see Figure 11 below). The location of the transition point is variable from simulation to simulation because the transition requires fluctuation of a certain size to occur. In the case of spontaneous pattern transitions between the F and the P patterns, either layer 5 or 4 can remain continuous (in Figure 10.F, layer 5 is continuous). In some cases neither layer is continuous.

The magnitude of developmental noise determines the variability of the point of spontaneous transition: the noisier the system, the more variable is this point. Larger noise will decrease the critical value of the peripheral field, above which a spontaneous transition can occur.

Possible developmental scenarios can be described in the following generalized view. Figure 11 illustrates the development of the LGN as a movement of a point along the x axis (which can also be considered the time axis) on a potential surface. For any given x, the system is described as being in a structural state (laminar or not) depending on the arrangement of the cells at this point. Each state has an associated energy, plotted along the vertical axis. The profile of the energy as a function of the state may change with x if the external fields change with x. If the initial state is in a potential well which remains sufficiently deep along x (in comparison to the developmental noise), the system will remain in this state for all x, even if there are lower energy states. The system may change its state for two possible reasons: 1) at some x the barrier between the two minima becomes too low relative to the noise; 2) an external perturbation induces a switch between the original and the new state. The former case is a spontaneous transition, the latter case is an induced one. A spontaneous transition will have a variable location in LGNs with the same parameters, while the induced transitions will always be at the position of the perturbation that triggers the transition. The results presented so far confirm that the perturbation in retinotopy, caused by the optic disk gaps, can serve as the external impetus inducing a state transition.

not clear if we need this figure

For any given energy profile there will be a critical size of the perturbation which can induce a transition. The critical size of the gaps is of the same order of magnitude as the interaction distance, σ, and depends on the layer thickness, as well as on the relative magnitudes of the internal, foveal and peripheral fields. These parameters are related to the critical gap size

in the following way: an increase of layer thickness, interaction distance, cell density[14], or magnitude of the foveal fields at the location of the gaps, increases the critical gap size; an increase of the peripheral fields decreases the critical gap size.

In all three-dimensional simulations described below the values of the parameters used are: $S_x = 10$, $S_y = 10$, $S_z = 6$, $N = 4800$ cells (which translates to a cell density $\rho = 8\,\text{unit}^{-3}$).

3.3.1 System without Optic Disk Gaps

Simulation VII illustrates development of a three-dimensional LGN without optic disk gaps. Results of this simulation are presented in Figure 12. The external fields are of the same form as in Eqs. (14 and 15). The magnitude of the foveal fields is $A_f = 10$; the magnitude of the peripheral fields is $A_p = 5$; the rate of cell development is $\alpha = 10^{-4} \exp\left(-4\,(y - S_y)^2/S_y^2\right)$, i.e., the width of the Gaussian is half the system size along the y axis. In Figure 12.A one can see that the shape of the wave front follows closely the form of the rate of development.

From Eqs. (17) one finds that for $x < x_c$, where $x_c = \ln\left(A_f/A_p\right) = \ln 2$, the foveal fields dominate, while for $x > x_c$ the peripheral fields dominate. Patterns F and P will then be favored for $x < x_c$ and $x > x_c$, respectively. As for the two-dimensional model, the internal fields created by already maturing cells are strong enough to stabilize the F pattern even for $x > x_c$ (see Figures 12.B and 12.C). Once created in the foveal representation, the F pattern can propagate through the whole system, although, almost everywhere this pattern is a metastable state. Of course, if the peripheral fields were always smaller than the foveal ones, the F pattern would propagate even more easily. Figure 12.D shows a cut through the system at $y = S_y/2$ to illustrate the homogeneity of the mature state of the LGN.

Similarly to the two-dimensional LGN, organization into projection columns plays a decisive role stabilizing laminar patterns and allowing a smooth

[14]The cell density and the interaction distance as shown earlier determine the magnitude of the internal field.

"propagation of sameness". Naturally, if the peripheral fields exceed a certain magnitude the F pattern will not propagate everywhere. A transition to the favored P state will occur at some time during development. The critical value, A_p^c, of the peripheral field, above which a spontaneous transition to the P pattern occurs, depends on the values of the cell density, interaction distance, layer thickness and magnitude of the foveal fields. The larger any of these parameters, the larger is the critical magnitude of the peripheral field. For the parameters used in the described simulation the critical magnitude is $A_p^c \approx 60$. An additional parameter, which influences the magnitude of the critical peripheral fields, is the width of the wavefront. The wider the wave is, the larger is A_p^c. This means that a developmentally "more three-dimensional" LGN is, in general, more stable. This observation is consistent with the fact that a wave with a wider wavefront propagates faster. Velocity of propagation is related to the magnitude of the internal field. When more cells participate in development, this field is larger. Therefore, the velocity is larger, and the system is more insusceptible to external influences.

Measured velocity of propagation of the F pattern (with no peripheral fields present) qualitatively follows the form predicted in [43]. Velocity has intermediate values between the values of velocities of ideal two- and three-dimensional systems, and is larger for wider waves, denser systems, or when the cell-cell interaction has longer range.

3.3.2 System with Optic Disk Gaps – Induced Transition

The optic disk in the contralateral retina is modeled in Simulation $VIII$ by restricting the cells of some projection columns to only positive values of the eye specificity variable. Figure 13 presents results of the development of a three-dimensional LGN with square[15] gaps of size $g = 1$. The left edges of the gaps are at $x_g = 4$. All other parameters are the same as in the previous system with the exception of the width of the developmental wavefront, which is set to two length units. Figure 13.A shows the wave reaching the gaps. Layer 6 has just been able to establish its presence beyond the gaps. A cut in the middle of the LGN, along the x-axis, would appear as in Figure 10.A. Layer 4 is being squeezed out by layers 5 and 3 which are intruding into

[15]The dimensions of the macaque optic disk are approximately six by four degrees in horizontal and vertical planes, respectively. The gaps in the LGN have similar proportions, and can be well approximated as squares.

its gap (see also Figure 13.D). In Figure 13.B the developmental wave has reached the peripheral edge of the LGN. Sublayers 5 and 4 have exchanged places in the pattern at this edge.

Figure 13.C shows the final state of the LGN. It consists of two parts, the foveal part is in the F state; the peripheral part is in the P state. The boundary between the two parts consists of two planes meeting at an angle at the gaps (c.f. Figure **??** in [43]). Figure 13.D shows a cut through the mature nucleus along a middle line parallel to the x axis. The pattern transition is locked at the position of the gaps. Compare this picture with the anatomical reconstruction of the macaque LGN shown in Figure 3. The cells of type 6 and 4 are mixed in the layer 6+4; the cells of type 5 and 3 are mixed in layer 5+3 in the peripheral LGN part. The degree of mixing depends on the noise in the development and the magnitude of the peripheral fields. Stronger noise increases the mixing, while stronger fields suppress the mixing and preserve anatomically hidden substrata of ON and OFF cells in the merged peripheral layers.

The same parameters as in the two-dimensional model determine (in the same way) whether the gaps will trigger a pattern transition or not. The third dimension adds the width of the wavefront as an additional relevant parameter. The narrower the incoming wave, the easier a switch in the pattern can be induced. This is intuitively clear, since to a narrower wave the gaps appear larger than to a wider wave, and, therefore, constitute a stronger perturbation. The shape of the interface between the two patterns also depends on the wavefront width. Narrower waves produce transition surfaces shifted towards the foveal part of the nucleus, i.e., the angle between the two transition planes[16] at the gap depends on the wavefront width and the relative velocities of propagation of the F and the P patterns. This angle is larger when: the peripheral fields are stronger, the wavefront is narrower, and the cell density is smaller. The transition surfaces will run approximately perpendicular to the lateral edges (as in the macaque LGN) for many combinations of the values of the above parameters.

[16]Strictly speaking these surfaces are not planes, but they look sufficiently flat to be called planes.

As in the two dimensional model, it is possible to observe a spontaneous transition between the F and the P patterns. The condition for this is presence of a strong peripheral field which can overcome the stabilizing foveal and internal fields. In a system with gaps, they must be not a very strong perturbation for an incoming F state, otherwise they will induce an irreversible transition.

Results of Simulation IX, presented in Figure 14, illustrate this case. The values of most of the parameters in this simulation are the same as in Simulation $VIII$. The difference is that the gaps are moved to $x_g = 1.5$, the magnitude of the foveal field is $A_f = 100$, and the magnitude of peripheral fields is $A_p = 70$. Increasing the peripheral field magnitude to this value guarantees a spontaneous transition. The gaps are moved closer to the foveal end to allow more space for the transition to take place, and to illustrate the importance of the balance between the fields and the magnitude of the perturbation. Namely, at the position of the gaps the foveal fields are still sufficiently strong and the gap is a sufficiently weak a perturbation. This combination allows the F state to propagate past the gaps as shown in Figure 14.A.

In Figure 14.B the wave reaches the peripheral end. The transition between the F and P patterns has occurred at $x \approx 6.5$ but cannot be seen because the P pattern has not yet reached the lateral edges. Figure 14.C shows the final state of the LGN. The foveal part of it, which includes the optic disk gaps, is in the F laminar state; the peripheral part is in the P state. The boundary between the two parts consists of two planes meeting on the main axis and forming a sharp angle towards the foveal end. The reason for this is the much faster propagation of the P pattern in the presence of the strong peripheral fields. Figure 14.D shows a cut along the main axis. Note the gaps in layers 6 and 4. The spontaneous laminar transition has a different topology than that of the induced transition shown in Figure 13.D. The induced transition is associated with an interruption of sublayer 4, while this spontaneous transition involves an interruption of layer 5. Because the spontaneous transitions are not associated with any type of a geometrical perturbation either layer 4 or 5 can be interrupted while the other one remains continuous. Which layer will be continuous and which one will be

discontinuous is a random choice between two equally probable cases[17]. The exact position of a spontaneous transition is variable. The only restriction is that it cannot occur foveal to some point where the F and P states are equally stable and the energy barrier between them is too high[18]. A transition may occur anywhere peripheral to this point with increasing probability as the P state becomes more stable and the energy barrier between the F and the P state decreases.

4 Discussion

This work contains, to our knowledge, the first computational model of the morphogenesis of a brain structure to capture key features in a biologically realistic framework. It considerably strengthens the hypothesis that the optic disk gaps are causally related to the laminar transition, that is, that they trigger the transition in its usual position. The model incorporates two major features lacking in earlier work: the three-dimensionality of the LGN, and the wave of laminar development that occurs during morphogenesis. The model reveals that a transition associated with essentially a point singularity can propagate across the entire LGN. Investigations of the LGN structure in other primates, chimpanzee and human, that we are currently carrying on, show that the transition and gaps co-localize in these species too, which greatly diminishes the counter argument that these features coincide in rhesus by chance. Only full three-dimensional reconstruction of the LGN structure will answer this question unambigously.

The model lends itself to a future interplay between neurobiology and neural modeling in which one can examine biological tissue for the mechanisms underlying some of the parameters in the model, and use those that appear promising to further refine the model. For example, interaction distances might be determined by the dimensions of axonal or dendritic arborization. It might be productive to see if these vary with distance from the fovea, something that is not known for retinal axons and geniculate dendrites.

[17]The example of a spontaneous transition in a two-dimensional system shown in Figure 10.F has a continuous layer 5 and a discontinuous layer 4.

[18]A large fluctuation in the system which might potentially switch the state would destroy the laminar structure, and in some extreme cases might even prevent propagation of a smooth developmental wave.

The proposed model is sufficiently detailed and can be experimentally tested. For example, the model predicts that a hole in the contralateral retina more foveal (but not too foveal) than the optic disk, lying on the horizontal meridian, would cause a "premature" transition in the LGN passing through the image of this artificial hole. Experiments have been reported, in which a macaque fetus is surgically removed from the mother before the LGN development starts, enucleation of one eye is performed, and the fetus is put back, leading to a normal delivery[35, 36]. In a similar operation one might punch a hole in the retina (for example with a UV laser) without removing the eye, and return the fetus. After birth, the LGN structure could then provide a test of the model. In such an experiment, the major problem would probably be the healing of the artificial hole in the retina. It may not be impossible to find individuals with natural retinal holes. The exact shape of the transition surface could also serve as a test of the model. However, one needs to further advance the analysis of the model dynamics and include more detailed information on the LGN geometry and the spatial distribution of the cell density. It is also feasible that the velocity of the developmental wave be measured, and its dependence on the cell density compared with the predictions.

Ideally, one would want to simulate the whole LGN using a "microscopic" model with detailed information about synapses between all RG and LGN cells, and with realistic monotonic external morphogenetic gradients. Such a simulation will remove the most "unbiological" features of the model. However, even in the present formulation the model provides the intuition how the a singularity in the retinotopic map can act as a seed for the transition surface separating the two laminar patterns.

The model system provides a good example of the importance of seemingly minor morphological features in biology. One need not always assume that the cause has the same magnitude as the effect.

References

[1] A. Antonini & M. P. Stryker (1993) Rapid remodeling of axonal arbors in the visual cortex. *Science,* **260:** 1819-1821.

[2] W. Burke & A. M. Cole (1978) Extra-retinal influences on the lateral geniculate nucleus. *Rev. Physiol., Biochem., and Pharmacol.,* **80:** 105-166.

[3] P. Collet, & J.-P. Eckmann. *Instabilities and Fronts in Extended Systems.* Princeton University Press, Princeton, New Jersey, 1990

[4] M. Conley & D. Fitzpatrick (1989) Morphology of retinogeniculate axons in macaque. *Vis. Neurosc.,* **2:** 287-296.

[5] A. Dekaban (1954) An anatomical, developmental and pathological study. Development of the human thalamic nuclei, *J. Comp. Neurol.,* **100:** 63-97.

[6] E. A. DeYoe & D. C. Van Essen (1988) Concurrent processing streams in monkey visual cortex. *Trends Neurosci.,* **11:** 219-226.

[7] J. E. Dowling. *Neurons and Networks.* Belknap Press, Cambridge, 1992.

[8] M.S. Gilbert (1934) The early development of the human diencephalon, *J. Comp. Neurol.,* **62:** 81-116.

[9] R.W. Guillery. (1975) Retinal representations, *Science,* **267:** 1038.

[10] D. Hebb. *The Organization of Behavior; a Neuropsychological Theory.* Wiley, New York, 1949.

[11] A. Hendrickson & P. Rakic (1977) Hystogenesis and synaptogenesis in the dorsal lateral geniculate nucleus (LGd) of the fetal monkey brains, *Anat. Res.,* **187:** 602 (Abstract).

[12] T.L. Hickey & R.W. Guillery. (1979) Variability of Laminar Patterns in the Human Lateral Geniculate Nucleus, *J. Comp. Neurol.,* **183:** 221-246.

[13] P.F. Hitchcock & T.L. Hickey (1980) Prenatal development of the human lateral geniculate nucleus, *J. Comp. Neurol.,* **194:** 395-411.

[14] D. Hubel. *Eye, Brain, and Vision.* W. H. Freeman & Co., New York, 1988.

[15] D. H. Hubel & T. N. Wiesel (1965) Binocular interaction in striate cortex of kittens reared with artificial squint. *J. Neurophysiol.,* **28:** 1041-1059.

[16] J.H. Kaas, R.W. Guillery & J.M. Allman. (1972) Some principles of organization in the dorsal lateral geniculate nucleus, *Brain Behav. Evol.,* **6:** 253-299.

[17] E. R. Kandel, J. H. Schwartz, T. M. Jessell. *Principles of Neural Science.* Springer-Verlag, Berlin, 1991.

[18] S. W. Kuffler (1957) Discharge patterns and functional organization of mammalian retina, *J. Neurophysiol.,* **16:** 37-68.

[19] M. M. La Vail, D. H. Rapaport & P. Rakic(1991) Cytogenesis in the monkey retina. *J. Comp. Neurol.,* **309 (1):** 86-114.

[20] D.Lee & J.G.Malpeli. (1994) Global Form and Singularity: Modeling the Blind Spot's Role in Lateral Geniculate Morphogenesis, *Science,* **263:** 1292-1294.

[21] S. LeVay, T. N. Wiesel & D. H. Hubel (1980) The development of ocular dominance columns in normal and visually deprived monkeys. *J. Comp. Neurol.,* **191:** 1-51.

[22] S. LeVay, M Connoly, J. Houde & D. C. Van Essen (1985) The complete pattern of ocular dominance stripes in the striate cortex of the macaque monkey. *J. Neurosci.,* **5:** 486-501.

[23] M. W. Levine, J. M. Shefner. *Fundamentals of Sensation and Perception.* Brooks/Cole Publishing Company, Pacific Grove, 1991.

[24] M. S. Livingstone & D. H. Hubel (1981) Effects of sleep and arousal on the processing of visual information in the cat. *Nature,* **291:** 554-561.

[25] M. S. Livingstone & D. H. Hubel (1988) Segregation of form, color, movement, and depth: Anatomy, physiology, and perception. *Science,* **240:** 740-749.

[26] J.G. Malpeli & F.H. Baker. (1975) The representation of the visual field in the lateral geniculate nucleus of Macaca mulatta, *J. Comp. Neurol.,* **161:** 569-594.

[27] J.G. Malpeli, D. Lee & F.H. Baker. (1993) Eccentricity-related variations of magnocellular and parvocellular inputs to Macaque striate cortex, *Invest. Ophthal. and Vis. Sci.*, **34:** 812.

[28] D. N. Mastronarde (1989) Correlated firing of retinal ganglion cells. *Trends in Neurosc.*, **12:** 75-80.

[29] M. Meister, R. Wong& D. Baylor(1991) Synchronous bursts of action potentials in ganglion cells of the developing mammalian retina. *Science,* **252:** 939-943.

[30] J.D.Murray. *Mathematical Biology.* Springer-Verlag, Berlin, 1989

[31] N. Okamura (1957) On the development of the medial and lateral geniculate body in man. *Arb. aus. der zweiten Abteilung des anatomischen. Institutes der Universitat zu Tokushima,* **2:** 129-216.

[32] D. Purves & J. Lichtman *Principles of Neural Development.* Sinauer Associates, Inc., Sunderland, MA, 1985

[33] P. Rakic. (1977) Genesis of the dorsal lateral geniculate nucleus in the rhesus monkey: site and time of origin, kinetics of proliferation, routes of migration and pattern of distribution of neurons, *J. Comp. Neurol.,* **176:** 23-52.

[34] P. Rakic. (1977) Prenatal development of the visual system in rhesus monkey, *Phil. Trans. R. Soc. Lond. B.,* **278:** 245-260.

[35] P. Rakic (1981) Development of visual centers in the primate brain depends on binocular competition before birth. *Science,* **214:** 928-931.

[36] P. Rakic (1986) Mechanism of ocular dominance segregation in the lateral geniculate nucleus: competitive elimination hypothesis. *Trends Neurosci.,* **9:** 11-15.

[37] R. Robb. *Analyze, Reference Manual, version 7.5,* Mayo Foundation, 1995.

[38] P.H. Schiller & J.G. Malpeli. (1978) Functional specificity of LGN of rhesus monkey, *J. Neurophysiol.,* **41:** 788-797.

[39] C. J. Shatz (1990) Competitive interactions between retinal ganglion cells during prenatal development. *J. Neurobiol.,* **21:** 197-211.

[40] M. P. Stryker & W. Harris (1986) Binocular impulse blockade prevents the formation of ocular dominance columns in cat visual cortex. *J. Neurophysiol.,* **6:** 2117-2133.

[41] S.Tzonev, K. Schulten, J. Malpeli. (1994) A Three-Dimensional Model of Rhesus LGN Morphogenesis: Interactions of the Blind Spot with a Wave of Development, Soc. Neurosci. Abstr., **20:** 135.

[42] S.Tzonev, J. Malpeli, K. Schulten. Morphogenesis of the Lateral Geniculate Nucleus: How Singularities Affect Global Structure, in *Advances in Neural Information Processing Systems 7,* G. Tesauro, D. Touretzky, J. Alspector eds., MIT Press, Cambridge, MA, 1995

[43] S.Tzonev, J. Malpeli, K. Schulten. in preparation.

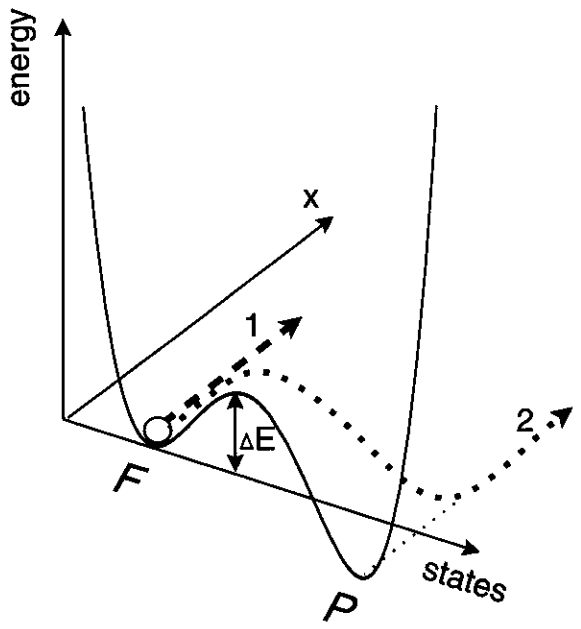

Figure 11:
A schematic representation of the development of the LGN as a movement of a point on an energy surface. The energy is a function of the state at any given x. The energy profile changes along the x axis when the external fields change. The system may stay in the same state along the x axis when the current state is a deep enough potential well, path 1. Fluctuations may produce a spontaneous transition when they are comparable to the energy barrier ΔE. The system may also move to a more stable state if it is perturbed by wide enough gaps, path 2.

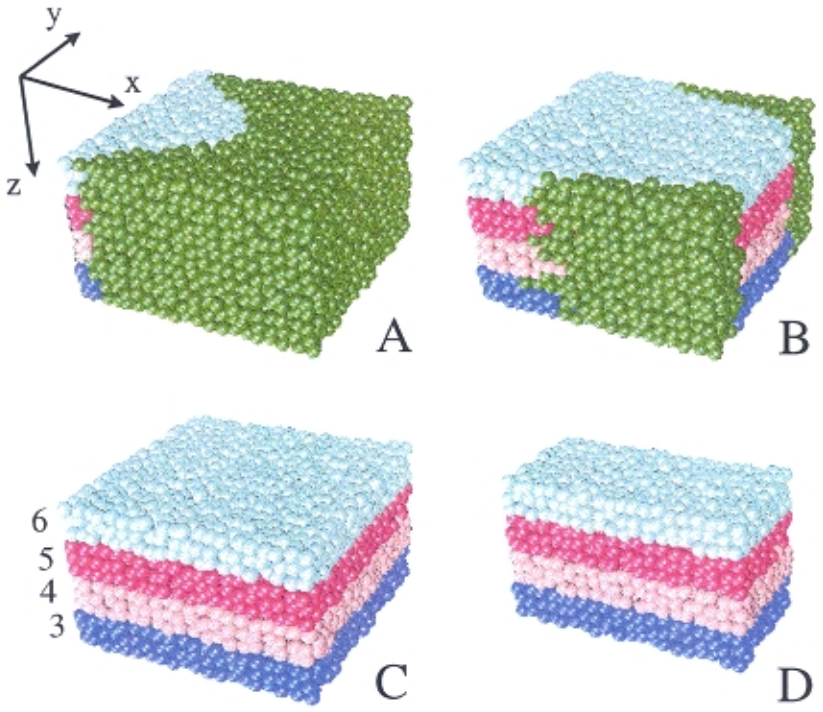

Figure 12: Development of a three-dimensional system without blind spot gaps, Simulation VII. **A**: Cells in the foveal end (close to $x = 0$) begin to acquire functionality. Cells are represented as colored spheres. The color codes for the cell functional properties. Darkest color means undeveloped ($|e_i| = |p_i| \leq 0.1$) cells. **B**: The wave of development reaches the peripheral end of the nucleus. Some cells are still undeveloped. **C**: Cells in the whole system have acquired functional properties. The foveal pattern has propagated throughout the nucleus. Types of cells comprising the layers are shown on the left. **D**: A cut of the nucleus at $y = S_y/2$ to show the homogeneity of the final pattern.

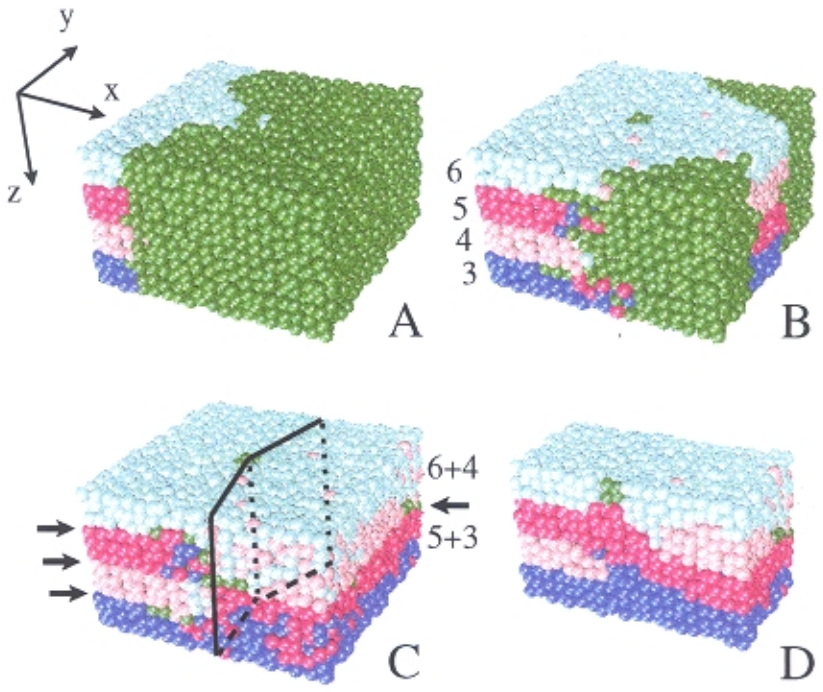

Figure 13: Development of a three-dimensional system with blind spot gaps in layers 6 and 4, Simulation *VIII*. The coding scheme is the same as in the previous figure. **A**: The developmental wave starts from the foveal end and has just jumped over the gaps. Only the gap in layer 6 is visible. **B**: The wave reaches the peripheral end of the nucleus. Note the switch between 5 and 4 sublayers. **C**: Most cells have reached their mature state. Some cells in the interlaminar positions and within the optic disk gaps do not have well defined functionality. Note the redistribution of cells of types 6 and 5, and 4 and 3 into two instead of four separate layers. The arrows indicate the position of the interlaminar spaces in the macaque LGN (Figure 3). The interface between the foveal and the peripheral patterns consists of two planes meeting at the location of the gaps. **D**: A cut of the nucleus at $y = S_y/2$. The switch between the two patterns coincides with the gaps. The gap in layer 4 is filled by cells of type 5 and 3.

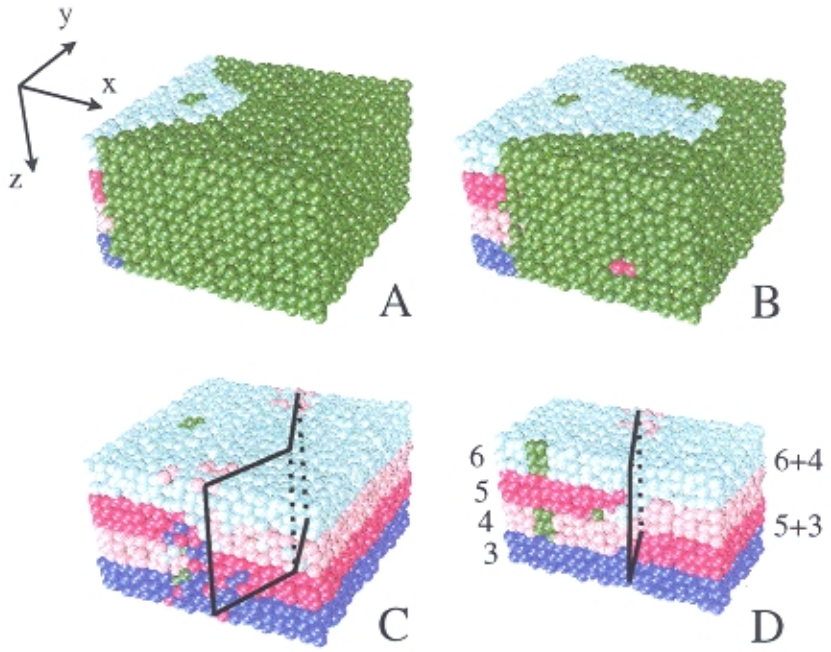

Figure 14: Results of Simulation IX: development of a three-dimensional system in which the optic disk gaps in layers 6 and 4 do not trigger a laminar transition because at their location the F state is still the most stable one. A spontaneous transition to the P state occurs beyond the gaps at a point where the peripheral fields are sufficiently stronger than the foveal ones. **A**: The developmental wave started in the foveal end has jumped over the gaps ($x_g = 1.5$) and is still propagating the F laminar pattern. **B**: The wavefront is approaching the peripheral end of the LGN. The transition from F to P state has occurred on the main axis but is not visible because the P pattern has not reached the lateral edges. **C**: Final state of the LGN. The transition surface consist of two planes meeting at the main axis and forming a sharp angle facing the foveal end. **D**: A cut through the nucleus at $y = S_y/2$. Note that in this transition layer 4 is continuous while layer 5 is interrupted.